

**Preliminary Finite Element Analysis
of a Compressor Disk in the
TF30 Engine**

J.S. Faragher and R.A. Antoniou

DSTO-TR-0915

DISTRIBUTION STATEMENT A
Approved for Public Release
Distribution Unlimited

20000216 007

Preliminary Finite Element Analysis of a Compressor Disk in the TF30 Engine

J.S. Faragher and R.A. Antoniou

Airframes and Engines Division
Aeronautical and Maritime Research Laboratory

DSTO-TR-0915

ABSTRACT

AMRL has been developing expertise in finite element analysis (FEA) of engine components, particularly compressor and turbine discs. The fourth stage Low Pressure Compressor (LPC) disc of the TF30 engine in the F-111 aircraft was chosen as the first component for detailed analysis after being identified as a prime candidate for the retirement-for-cause lifting methodology. This report describes a preliminary study of the stresses in this component. Two benchmark examples which show close agreement between FEA stress results and analytical solutions are presented. The FEA results confirm the critical location for low cycle fatigue failure specified by the OEM. The assembly loads are shown to significantly increase the mean and peak stresses but not the cyclic stress range. The thermal stresses are shown to be an order of magnitude smaller than the stresses caused by the rotation of the disc. The analysis shows that the most severe stresses produced in the disc under typical engine operating conditions are much lower than the yield stress of the disc material (Ti-8-1-1), which suggests a very conservative design. Recommendations are made for developing models that will more realistically represent the loads on the disc and the interaction with other components in order to determine whether the design is really as conservative as the current analysis suggests.

RELEASE LIMITATION

Approved for public release



Published by

*DSTO Aeronautical and Maritime Research Laboratory
PO Box 4331
Melbourne Victoria 3001 Australia*

*Telephone: (03) 9626 7000
Fax: (03) 9626 7999
© Commonwealth of Australia 2000
AR-011-166
January 2000*

APPROVED FOR PUBLIC RELEASE

Preliminary Finite Element Analysis of a Compressor Disk in the TF30 Engine

Executive Summary

AMRL is currently developing a capability to provide technical support to the RAAF in engine component life management. One focus of this work is the TF30 engine in the F-111 aircraft which is planned to continue in service up to the year 2020. As the RAAF is now the sole operator of the F-111 aircraft and the TF30-109 engine in the world the availability of technical support and spare parts from both the OEM and other countries is severely limited.

Engine components may be retired after a fixed number of hours under the "safe-life" method, or when a crack exceeding a prescribed length is found under the "retirement-for-cause" method. For both these lifting methods an essential part of engine component life management is the determination of the mechanical and thermal stresses in the components during engine operation. AMRL has therefore been developing expertise in finite element analysis (FEA) of engine components, particularly compressor and turbine discs. The fourth stage Low Pressure Compressor (LPC) disc of the TF30 engine was chosen as the first subject for detailed analysis after being identified as a prime candidate for the retirement-for-cause lifting methodology. This report describes a preliminary study of the stresses in this component. Two benchmark examples which show close agreement between FEA stress results and analytical solutions are presented. The FEA results confirm the critical location for low cycle fatigue failure specified by the OEM. The assembly loads are shown to significantly increase the mean and peak stresses but not the cyclic stress range. The thermal stresses are shown to be an order of magnitude smaller than the stresses caused by the rotation of the disc. The analysis shows that the most severe stresses produced in the disc under typical engine operating conditions are much lower than the yield stress of the disc material (Ti-8-1-1), which suggests a very conservative design. Recommendations are made for developing models that will more realistically represent the loads on the disc and the interaction with other components in order to determine whether the design is really as conservative as the current analysis suggests.

The results of this analysis will assist the RAAF in making decisions about the life management of this engine component.

Authors

J.S. Faragher Airframes and Engines Division

John Faragher obtained a B.E.(Hons) from the University of Melbourne in 1987. He commenced work in the Propulsion Research Area at the Defence Science and Technology Organisation's Aeronautical and Maritime Research Laboratory in 1988. He worked in the areas of Engine Performance and Engine Mechanical Integrity. He was awarded a cadetship to study full-time at the University of Melbourne from 1992 to 1995 and was awarded a Ph.D. (Engineering). Since 1995 he has continued to work in the Propulsion Research Area at the Aeronautical and Maritime Research Laboratory and has been involved with the development of experimental facilities and finite element computer models for research into gas turbine engine temperature prediction, heat transfer problems and stress analysis.

R.A. Antoniou Airframes and Engines Division

Ross Antoniou is currently a Senior Research Scientist in the Propulsion Research Area of AED. He joined AMRL in 1990 after obtaining a Ph.D. from the University of Melbourne in 1988 and has worked in the areas of performance of advanced materials and coatings for transmission and propulsion systems, fatigue and fretting-fatigue behaviour, fracture and tribological behaviour. Currently he is working in the area of Engine Component Life Management with particular emphasis on component lifting methodologies, engine material behaviour, fatigue crack growth modelling, stress analysis and creep analysis.

Contents

| | |
|---|-----------|
| 1. INTRODUCTION..... | 1 |
| 2. BACKGROUND | 2 |
| 2.1 Retirement-For-Cause (RFC)..... | 2 |
| 2.2 Component Selection For RFC | 2 |
| 2.3 The TF30 Engine..... | 3 |
| 3. FINITE ELEMENT ANALYSIS OF THE DISC..... | 3 |
| 3.1 Benchmark Analyses | 3 |
| 3.2 Analysis of the fourth stage LPC disc of the TF30 engine | 4 |
| 3.3 Mesh | 4 |
| 3.4 Loads and Boundary Conditions | 5 |
| 3.4.1 Load Cases..... | 5 |
| 3.4.2 Constraints | 5 |
| 3.4.3 Centrifugal Load on Disc and Blades | 6 |
| 3.4.4 Interference Fit Load | 6 |
| 3.4.5 Temperature Field | 6 |
| 3.5 Results | 7 |
| 3.5.1 Results for Selected Locations on the Disc | 7 |
| 3.5.2 Results for Loads Applied Individually (cases 1 to 6) | 7 |
| 3.5.3 Results Simulating an Operating Engine (cases 7 to 10)..... | 8 |
| 3.5.4 Stress Range at the Snap Fillet Radius for Major Engine Usage Cycles | 9 |
| 3.5.5 Detailed Stress Results for the Snap Fillet Radius | 9 |
| 3.6 Discussion of FEA Results | 10 |
| 4. EXPERIMENTAL VALIDATION OF FEA MODEL..... | 11 |
| 4.1 FEA of Tension Test Specimen | 11 |
| 4.2 Fatigue Tests | 11 |
| 4.3 Fractography..... | 11 |
| 4.4 FAST | 12 |
| 5. CONCLUSIONS AND RECOMMENDATIONS..... | 13 |
| 6. ACKNOWLEDGMENTS | 14 |
| 7. REFERENCES | 14 |
| APPENDIX 1 BENCHMARK EXAMPLES | 33 |

List of Abbreviations

| | |
|------|--|
| FEA | finite element analysis |
| FAST | Focal-plane Array Synchronous Thermography |
| LP | low pressure |
| LPC | low pressure compressor |
| HP | high pressure |
| IDLE | flight idle power setting of the engine |
| MIL | military power setting of the engine (maximum without afterburner) |
| OEM | original equipment manufacturer |
| PWA | Pratt & Whitney Aircraft |
| RAAF | Royal Australian Air Force |
| RFC | Retirement for Cause |
| USAF | United States Air Force |

Nomenclature

| | |
|---------------|--------------------------------|
| σ_{xx} | x component of stress [ksi] |
| σ_{yy} | y component of stress [ksi] |
| σ_{zz} | z component of stress [ksi] |
| σ_1 | maximum principal stress [ksi] |
| σ_2 | middle principal stress [ksi] |
| σ_3 | minimum principal stress [ksi] |

1. Introduction

AMRL is currently developing its capability to provide technical support to the RAAF in engine component life management. One focus of this work is the TF30 engine in the F-111 aircraft, which is planned to continue in service up to the year 2020. As the RAAF is now the sole operator of the F-111 aircraft and the TF30-109 engine in the world the availability of technical support and spare parts from both the OEM and other countries is limited.

One essential part of engine component life management is the determination of the mechanical and thermal stresses occurring in the components during operation. AMRL has therefore been developing capability in using the finite element method for stress analysis of engine components, particularly compressor and turbine discs. The fourth stage Low Pressure Compressor (LPC) disc of the TF30 engine was chosen as the first component for detailed analysis after being identified as a prime candidate for the retirement-for-cause lifting methodology[1].

Important activities in order to achieve the objectives are:

1. Estimation of the principal stresses in the fourth stage LPC disc and the variation of these stresses with a range of assembly loads and engine speeds.
2. FEA determination of the radial stress in the disc for use in simple tension fatigue tests of specimens cut from the disc, and the use of these fatigue tests to validate the FEA prediction of the failure location in the specimen.
3. Evaluation of the FAST experimental technique as a tool for the qualitative validation of FEA stress field predictions and the prediction of likely failure locations.

This report describes a study of the stresses in this component using both numerical and experimental techniques. Section 2 presents the background to the work. Section 3 describes the finite element analysis of the disc using a two-dimensional axisymmetric model. Section 4 compares experimental fatigue test results with the prediction of the failure location from a three-dimensional finite element model of the test specimen. In Section 5 qualitative stress field results obtained with the Focal-plane Array Synchronous Thermography experimental technique are presented. Section 6 gives the conclusions and recommendations for further work. Two benchmark finite element stress analyses for simple rotating disc profiles, which were performed to develop confidence in the application of the analysis method to rotating discs, are presented in the Appendix.

2. Background

2.1 Retirement-For-Cause (RFC)

To avoid catastrophic failure caused by low cycle fatigue the rotating components of the TF30 engine are retired under a safe life methodology after a fixed number of engine operating hours. Under this conservative methodology 99.9% of components would not be expected to contain detectable cracks when they are retired. An alternative method for life management of engine components is Retirement for Cause (RFC) [2]. Under this method components are inspected at designated intervals and, if no cracks are found which exceed the allowable limit, they are returned to service. This lifting method has been used very successfully by the USAF with the F-100 engine in F-15 and F-16 aircraft. Australia is investigating the feasibility of RFC as an economical strategy for maintaining certain TF30 engine components in service for another twenty years. Implementation of RFC may even make it feasible to use second-hand engine components with unknown usage histories.

An integral part of RFC is the determination of crack initiation and propagation times. These are dependent on the cyclic stresses experienced by a component. Therefore the ability to identify the critical locations in turbine and compressor discs and predict the thermal and mechanical stresses at these locations is of fundamental importance.

2.2 Component Selection For RFC

At a meeting of RAAF and DSTO staff at RAAF Base Amberley in May 1997 potential RFC candidate components in the TF30 engine were assessed against the following criteria: [1]

- Part has limited, but not critically short life (Say, 4000 - 6000 hours).
- Single (or at most two) life limiting locations.
- Relatively expensive replacement cost (above \$5000).
- Parts are likely to exceed stated "Throw Away" lives by the year 2020.
- Only P-109(RA) configuration parts to be included in the study.

The following four TF30 engine components were identified as the best candidates for RFC:

- 3rd Stage Fan Disc.
- 4th Stage Low Pressure Compressor Disc.
- 2nd Stage Low Pressure Turbine Disc.
- 4th Stage Low Pressure Turbine Disc.

From this list the 4th Stage Low Pressure Compressor (LPC) disc was chosen as the first subject for detailed analysis (Figs. 1, 2, 3 and 4). This disc has a snap, which is a circumferential protrusion about one third of the distance between the bore and the rim of the disc. It provides a surface which mates with the spacer-3-4 which connects

the 4th Stage LPC disc and the 3rd Stage Fan disc. An inwards radial load is exerted on the snap by the spacer-3-4, which has a slightly smaller diameter, and it is assembled using differential heating before being bolted together. The allowable tolerance range on the difference between the spacer-3-4 diameter and the snap diameter is 0.0 - 0.0045".

The critical low-cycle fatigue location specified by Pratt & Whitney Aircraft (PWA) for this disc is the front snap fillet radius. This location is in the corner where the front surface of the disc and the load bearing surface of the snap, which is normal to it, meet as shown in the schematic diagram in Figure 4. The allowable tolerance on the snap fillet radius is 0.008" - 0.018". The disc retirement life promulgated by PWA is a function of the snap fillet radius dimension. This relationship is illustrated in Figure 5 [3] where the snap fillet radius varies from 0.008" - 0.018" and the corresponding retirement life varies from 1500 - 15000 hours. The analysis described in this report is for a snap fillet radius dimension of 0.013". It is relevant to note that routine inspections at overhaul have never found evidence of cracking in the snap fillet radius of this disc. The disc was designed in 1960's when less sophisticated analysis tools were available, so the design is probably very conservative.

2.3 The TF30 Engine

The TF30 engine is a two-spool turbo-fan engine with afterburner. The three-stage fan and six stage low-pressure (LP) compressor are driven by a three stage LP turbine. The seven stage high-pressure (HP) compressor is driven by a single stage HP turbine.

At Military Power (maximum power without afterburner) the LP spool rotates at 10,000 rpm and the HP spool rotates at 14,500 rpm, and the engine produces 12,000 lbs thrust. Maximum thrust with afterburner for the -109 version of the engine is 20,840 lbs.

3. Finite Element Analysis of the Disc

3.1 Benchmark Analyses

To develop confidence in the application of the finite element stress analysis method to rotating discs two benchmark analyses were performed. These finite element stress analyses were then compared with analytical solutions for simple rotating disc profiles and are presented in the Appendix.

The agreement between the finite element predictions and the analytical results for these simple benchmark geometries is very good (typically within 3%). This confirmed that the finite element software was correctly applied to the rotating disc configuration

and provided a foundation on which to base the application of the method to the gas turbine compressor disc.

3.2 Analysis of the fourth stage LPC disc of the TF30 engine

A linear elastic finite element analysis of the fourth stage LPC disc of the TF30 engine was performed using Patran (version 7.5 - 8.1) for pre- and post-processing and using Abaqus (version 5.6 - 5.8) as the solver running on a Hewlett Packard K series 9000 computer at AMRL. Only the fourth stage LPC disc itself was included in this preliminary finite element model. The spacers, air seal, tie rods and tie rod sleeves were not included. Non-axisymmetric features, such as the reduced amount of material in the bolt circle, were not included in the model or compensated for. Imperial units have been used throughout for compatibility with existing OEM data.

The use of two-dimensional axisymmetric solid elements to model a cross-section of the disc implicitly simulates the behaviour of the three-dimensional axisymmetric structure of the disc. The loads acting on the disc are also axisymmetric. These comprise the centrifugal force acting on the disc and the blades caused by the rotation of the disc, the load on the front snap caused by an interference fit with the spacer-3-4, and the thermal stresses caused by the non-uniform temperature of the disc. Two speeds of rotation were included in the analysis: 5,000 rpm which corresponds to the IDLE power setting and 10,000 rpm which corresponds to the MIL (military) power setting.

The disc is made of Ti-8-1-1 (specification PWA-1202). The material properties used in the analysis were assumed to be independent of temperature although, in reality, the material properties of Ti-8-1-1 vary with temperature. The assumed properties were:

Young's modulus = 17,200,000 psi

Poisson's ratio = 0.33

Density = 0.000404 lbf s²in⁻⁴

Coefficient of thermal expansion = 5×10^{-6} °F⁻¹

Reference temperature = 68 °F

The geometry of the cross-section of the fourth stage LPC disc was taken from a Pratt & Whitney Aircraft drawing (Figure 3) [4]. The geometry was created in AutoCAD (version 13) and imported into Patran in IGES format.

3.3 Mesh

The geometry of the disc was meshed almost entirely using 8-node biquadratic axisymmetric 2-dimensional solid elements. A small number of 6-node quadratic axisymmetric elements were also used. Figure 6 shows the complete mesh comprising 519 elements. A coarse mesh was used near the rim and bore of the disc because precise stress results were not a major concern in these areas. A fine mesh was used in

the region of interest around the front snap fillet radius. The accuracy of using six elements around the snap fillet radius is discussed in section 3.4. Figure 7 shows the snap fillet radius with element and node numbers. The disc was only meshed in the radial direction as far as the live rim, i.e. the base of the blade slots. To simulate the centrifugal load acting on the excluded blade posts and blades a pressure load was applied to the live rim of the disc (see section 3.2.2).

Solely for the purpose of visualization the mesh was swept by 90° in an anti-clockwise direction about the centre of rotation (y-axis) to produce a three-dimensional picture of the disc as shown in Figure 8. This picture gives a clearer indication of what the mesh in Figure 6 is actually modelling. Figure 8 also shows how the two-dimensional mesh was positioned to obtain the correct orientation relative to the global coordinate system for an axisymmetric model. This requires that the cross-section of the disc lies in the x-y plane, the y-axis is the axis of rotation, the x-axis is the radial direction and the z-axis is the tangential (hoop) direction.

3.4 Loads and Boundary Conditions

3.4.1 Load Cases

Table 1 shows which of the loads were applied in each of the ten load cases for which results are presented in this report. The individual loads are described below. In cases 1 to 6 the individual loads were applied separately so that the individual stress results can be easily scaled and combined using linear superposition to produce results for different magnitudes and combinations of loads, if desired. The magnitudes of the individual loads applied to the finite element model are the best available estimates of the actual loads on the disc for the IDLE and MIL engine power settings within the assumptions of this analysis. Cases 7 to 10 provide results for combinations of the applied loads which simulate actual operation of the engine.

3.4.2 Constraints

In an axisymmetric model rigid body motion in the x and z directions does not need to be constrained because it is controlled by the definition of axisymmetric elements. However, one node must be constrained to prevent rigid body motion in the y direction - any node may be chosen. The initial results with only a single node at the bolt circle constrained showed excessive bending in the disc web regions, hence a second node at the bolt circle location was constrained in the y-direction to simulate the restraining influence of the spacers and tie rods on the disc. These two points are labelled A and B in Figure 9.

3.4.3 Centrifugal Load on Disc and Blades

The rotation of the disc and blades creates centrifugal forces. These forces were applied to the disc but as the blade posts and blades were not included in the model the effect of the centrifugal forces acting on these bodies had to be simulated by an equivalent pressure load acting on the live rim of the disc. The radial pressure load acting on the live rim of the disc as a result of the centrifugal load acting on the blade posts and blades was calculated to be 1099 psi for the IDLE speed of 5,000 rpm and 4397 psi for a disc speed of 10,000 rpm at Military Power (MIL) as shown in Figure 10. There is a slight offset of the rim of the disc by 0.014" in the y-direction from the disc web centreline which creates a bending moment.

3.4.4 Interference Fit Load

The spacer-3-4 was not included in the finite element model so the load acting on the front snap caused by the interference fit with the spacer-3-4 was simulated by a pressure load acting radially inwards (the negative x direction) on the front snap of the disc, as shown in Figure 9. The magnitude of this load was determined by a trial and error procedure to achieve an average radial displacement of the snap equal to half of the interference dimension (or overlap) between the flange of the spacer-3-4 and the snap surface. This is based on the assumption that the mating surfaces of the snap and the spacer are displaced by equal amounts when they are assembled using differential heating to achieve the interference fit. It also assumes that the displacement is independent of the other applied loads and neglects the effect on cyclic stress of load passing through this component. To simulate an interference equal to the maximum tolerance of 0.0045" on the diameter (and hence 0.00225" on the radius) a pressure load of 900 psi was required to achieve an inward radial displacement of the snap of 0.0011". Since the analysis was linear, to simulate an interference equal to the nominal (half the maximum) tolerance of 0.00225" on the diameter (and hence 0.001125" on the radius) a pressure load of 450 psi was required to achieve an inward radial displacement of the snap of 0.00055".

3.4.5 Temperature Field

Thermal stresses are created in the disc by differential expansion because the disc is not at a uniform temperature during operation. Although these stresses are much smaller in a compressor disc than in a turbine disc they still need to be quantified. Temperatures at three radial locations on the disc were obtained from PWA Temperature Survey Test Results [5] for IDLE and MIL power settings. These values are shown in Table 2. The temperatures in between these locations were determined by linear interpolation. The bore of the disc is hotter than the rim because ninth stage bleed air is fed back through the centre of the compressor rotor assembly to pressurise the number 1 bearing seal at the front of the engine. The temperatures in Table 2 correspond to ground level static conditions. Higher temperatures would be

experienced with forward speed as a result of ram compression and heating of the intake air.

3.5 Results

3.5.1 Results for Selected Locations on the Disc

The stress results for the disc for load cases 1 to 4 are summarised in Table 3. The results for load cases 5 to 8 are summarised in Table 4. The results for load cases 9 and 10 are summarised in Table 5. The results are presented for selected nodes at the locations on the disc shown in Figures 11 and 12. Even though the primary area of interest is the snap fillet radius the peak stress for certain load cases occurs outside this region, so results are also presented for the bore, inner web, outer web and rim of the disc. This gives a fuller picture of the behaviour of the disc.

The z direction is always one of the three principal stress directions because the model is axisymmetric. Therefore the other two principal stress directions lie in the x-y plane. The edges of the model represent the surfaces of the disc. At the edges of the model one principal stress direction is parallel to the edge and the other is normal to the edge. Where there is no applied load at an edge the stress normal to the edge is equal to zero in reality, however it may not be exactly equal to zero in the finite element analysis because the results are not calculated at the edge of an element but at integration points within the element and then extrapolated to the nodes at the edge of the element. Where there is a steep stress gradient across an element the results at the edge may not be accurately predicted and the mesh may need to be refined. This issue is discussed further in section 3.4.

3.5.2 Results for Loads Applied Individually (cases 1 to 6)

In case 1 the only applied load is the interference fit load on the front snap. The highest stress (11.6 ksi) occurs in the snap fillet radius because of the stress concentration caused by the fillet radius. The applied load on the front snap in case 2 is twice as large as that in case 1. Since this is a linear elastic analysis the pattern of the stress results in case 2 is identical to that in case 1 but the stress values are twice as large (23.3 ksi maximum).

In case 3 the centrifugal force acting on the disc and blades due to the rotation of the disc at 5000 rpm is the only load present. The radial stress is equal to zero at the bore, as expected, and equal to the blade load at the rim. The hoop stress is large at the bore and decreases to a smaller value at the rim as expected for a rotating annular disc (c.f. the benchmark examples in the Appendix). The highest stresses occur in the inner and outer webs (14.2 ksi maximum). This is due to bending of the disc in the x-y plane caused by the asymmetric geometry of the disc and the small offset of the blade and

rim centre of gravity in the y-direction from the centreline of the outer web. In spite of the absence of a load on the snap the stresses in the snap fillet radius are only slightly less than the peak stress in the disc.

The pattern of the stress results in case 4 is identical to that in case 3 but the stress values are four times as large (56.9 ksi maximum in the inner and outer webs) because the disc speed is twice as high and the centrifugal force is proportional to the square of the rotational speed. It is interesting to note that both the radial stresses and the hoop stresses created in the snap fillet radius by the rotation of the disc at MIL speed in case 4 are significantly greater than the stresses caused by the direct action of the load on the snap representing the maximum interference fit between the disc and the spacer in case 2.

The only load on the disc in case 5 is caused by the thermal expansion resulting from the applied temperature field. The absence of a load on the snap results in low stresses in the snap fillet radius (< 1 ksi). The stresses caused by the thermal expansion of the disc are small compared with the stresses seen in cases 1 to 4. The maximum stress is 1.4 ksi at the rim. The increase in temperature causes the whole disc to expand radially. The expansion of the hotter material at the bore is restricted by the cooler material at the rim. The net result is compressive radial stresses throughout the disc, compressive hoop stresses in the bore and inner web regions, and tensile hoop stresses in the rim, outer web, bolt circle and snap regions.

Case 6 has higher temperatures and higher temperature gradients than were present in case 5, and therefore higher stresses. As in case 5, the radial stresses are compressive across the whole disc. However in contrast to case 5 the hoop stress is tensile only in the rim, outer web and bolt circle regions, and the compressive stress at the bore and inner web regions extends to include the snap region. The largest thermal stress occurring in the disc in case 6 can be seen to be 5.6 ksi at the rim, which is roughly one tenth of the magnitude of the largest stress caused by the rotation of the disc in case 4.

3.5.3 Results Simulating an Operating Engine (cases 7 to 10)

The results for load cases 7 to 10, which simulate an operating engine, are summarised in Table 6. Case 7 simulates the loads on the disc in an engine running at the IDLE power setting with an intermediate degree of interference between the spacer and the snap. Significant stresses are seen in the inner and outer webs (13 ksi), as were seen in case 3 where only the centrifugal load was acting. However the addition of the moderate load on the snap (450 psi), which was not present in case 3, creates a greater stress in the snap fillet radius (20.8 ksi). When the load on the snap is doubled in case 8, to simulate the maximum interference fit, the maximum stress in the disc again occurs in the snap fillet radius and is increased to 32.1 ksi.

Case 9 simulates an engine running at MIL power. The load on the snap is the same as it was in case 7 but the speed of the disc is twice as high. This causes large stresses to occur in the thin inner and outer webs as a result of increased bending of the disc (54.4 and 55.4 ksi respectively) as was seen in case 4. However, the stress at the snap fillet radius (55.9 ksi) is still slightly higher than that in the webs. In case 10 there is a greater load on the snap than in case 9. Therefore even though there is a large stress at the front side of the outer web, similar in magnitude to that in case 9 (55.0 ksi), a significantly greater stress occurs in the snap fillet radius (60.2 ksi).

3.5.4 Stress Range at the Snap Fillet Radius for Major Engine Usage Cycles

Table 7 shows the predicted stress range occurring at node 3777 for the two major engine usage cycle types. Node 3777 was chosen as a representative node for which to present results because it is in the region of the snap fillet radius where the highest stresses tend to occur (see section 3.3.5). The results in Table 7 for the IDLE-MIL cycle are simply the difference between the results for case 7 and case 9 in Tables 4 and 5. This is the same as the difference between the results for case 8 and case 10 because the constant increase in the snap load between case 7 and case 8 does not affect the stress range but only the mean stress and peak stress. The results in Table 7 for the STOP-MIL cycle are the differences between the results for case 9 and case 1 in Tables 3 and 5 (which are the same as the differences between the results for case 10 and case 2).

3.5.5 Detailed Stress Results for the Snap Fillet Radius

The highest stress in the snap fillet radius does not always occur at the same node but varies with the load case. Figures 13 to 16 show the stresses at each node in the snap fillet radius for each load case. (Figure 7 shows the node numbers in the snap fillet radius.) These plots show the stress in the z direction (hoop) and the stress parallel to the free surface, both of which are principal stress directions as explained above. The third principal stress direction is normal to the free surface and the stress in this direction must be zero because there is no external force applied at the surface. The fact that the FEA results in Tables 3 to 5 do not show this stress to be zero is a numerical inaccuracy which was mentioned above in section 3.3.1.

For cases 1 and 2, where the only applied load is the load caused by the interference fit on the snap and the disc is not rotating, the maximum stresses in the snap fillet radius occur at node 3750. On the other hand, in cases 3 and 4, where there is no load applied to the snap and the only load is the centrifugal force created by the rotation of the disc, the maximum stresses in the snap fillet radius occur at node 3804. For the combined loads applied in cases 7 to 10 the maximum stresses in the snap fillet radius occur between these two locations at node 3777.

Figure 16 shows that the assembly load on the snap simulating the interference fit has very little effect on the hoop stress. Similarly, Figure 15 shows that the assembly load has much less effect than the centrifugal load on the principal stress parallel to the free surface.

3.6 Discussion of FEA Results

In this highly simplified model the load on the front snap caused by the interference fit between the spacer and the disc has no effect on the cyclic stress range for IDLE-MIL or STOP-MIL engine usage cycles; but it does increase the peak stress and the mean stress occurring in the snap fillet radius region.

The peak stress in the snap fillet radius caused by the load on the snap representing the maximum interference fit between the disc and the spacer is 23.3 ksi (in case 2). The peak stress in the snap fillet radius when the only applied load is the rotation of the disc at MIL speed is 53.7 ksi (in case 4). The peak stress in the snap fillet radius for the most severe load case studied is 60.2 ksi (in case 10).

The peak stresses predicted by the model for every location are well below the yield stress for Ti-8-1-1 which is 130 ksi. These stresses are lower than expected, which may result from the fact that the finite element model does not include the spacers which are bolted to the disc in reality and very simple assumptions have been used to model the loads arising from the interactions of these components.

To evaluate the accuracy of the finite element model the "discretization errors" were determined. Where two or more elements share a node each element will calculate a different stress result for the node. The stress difference is determined as the difference between the maximum and minimum contributor to each node. The discretization error at each node is equal to half the value of this stress difference divided by the value of the peak stress that occurs anywhere in the model. This provides a measure of the quality of the mesh and indicates the locations where the mesh needs to be refined. According to the National Agency for Finite Element Methods and Standards (NAFEMS) (U.K.) [8] discretization error values of less than five percent of the peak stress indicate that the mesh is satisfactory. A stress difference plot for the maximum principal stress component in load case 2 is shown in Figures 17 and 19. These plots show the highest value of the stress difference to be 3524 psi. The values of the maximum principal stress for load case 2 are shown on the contour plots in Figures 18 and 20. These figures show a peak stress value of 23,280 psi. Therefore the maximum discretization error occurring in the snap fillet radius region is

$$\frac{3524/2}{23280} \times 100 = 7.6 \text{ \%}.$$

This indicates that the mesh is reasonable but could be improved.

No attempt has been made to refine the finite element mesh, but it is anticipated that further refinement would make a small improvement to the accuracy of the stress results. This applies particularly in the important region of the snap fillet radius because the stress concentrating effect of the fillet radius causes a very steep stress gradient within the elements at the edge of the model (Figure 20).

Since the retirement life for the disc promulgated by PWA is a function of the snap radius dimension it would be fruitful to investigate the sensitivity of the stress results to this dimension and compare the results with the data in Figure 5 via the appropriate Ti-8-1-1 S-N curve (i.e. stress vs. cycles to LCF failure curve). This, however, is beyond the scope of this report.

4. Experimental Validation of FEA Model

The validation of the full FEA model was not possible as full-scale spin pit testing was not available. Consequently it was decided, in order to determine the quality of the FEA modelling process, that a simplified geometrical model be constructed and that its predictions be verified using fatigue testing, fractographic analysis and FAST. The simplified geometry consisted of a section of the 4th LPC disc, as per figure 21, that could be tested in both fatigue and FAST situations.

4.1 FEA of Tension Test Specimen

The 3D model of the specimen was generated by extrusion of the 2D mesh in Z direction. This neglects the curvature of the disc, however as it is such a small segment this does not cause large error. The model uses the same material properties as above, it was fixed at one end, and loaded in simple tension at the other end. The predicted failure location was in the inner web region and there did not appear to be any significant stress concentration in the vicinity of the snap radius.

4.2 Fatigue Tests

In order to validate the FEA prediction of the failure location, determine the magnitude of the failure stress and identify the crack morphology, a number of axial fatigue tests were conducted under ambient conditions. The results of these tests are shown in Table 8.

4.3 Fractography

The FEA predicted the failure location as being the inner web runout radius and this was confirmed by the axial fatigue testing. Figure 22 (a) shows the typical failure site in the region of the inner web runout radius.

4.4 FAST

FAST (Focal-plane Array Synchronous Thermography) was developed in AMRL [7] and, as the name suggests, makes use of a focal-plane array infra-red camera coupled with synchronous averaging techniques, to capture the minute temperature fluctuations of a structural component under cyclic load. Based on the phenomenon known as the thermoelastic effect, it may be shown that such temperature measurements are directly proportional to the amplitude of the sum of principal stresses $\sigma_1 + \sigma_2 + \sigma_3$ (called the bulk stress or first stress invariant). Consequently, FAST scans may be interpreted as maps of bulk stress distribution when a cyclic load is applied to the component which has the same geometry as the specimen used for fatigue testing and FEA modelling.

By its nature, the FAST technique provides a qualitative indication of the stress distribution at or near the surface, provided that the specimen loading is representative.

Figure 23 shows the FAST results from a series of compression tests with and without an interference fit. The results may be summarised as follows:

1. FAST did provide useful qualitative validation of the stress distribution calculated using FEA for the case with no interference fit load on the snap. For example, Figure 23(a) compares well with Figure 23(d) which shows FEA first stress invariant contour results for a specimen under a compressive load in the direction of its length and with no interference fit load on the snap.
2. FAST did not provide useful results for the cases with an interference fit load because it was not possible constrain the specimen in the lateral direction. Clearly the presence of the interference fit load on the front snap (Figures 23(b) and (c)) causes considerable out-of-plane bending in the inner web because the component is not supported laterally with spacers and tie-bolts, as it would be in an actual engine.
3. FAST did not detect the area of stress concentration in the region of the snap fillet radius because it is so localised (see Fig. 20), FAST having a maximum resolution of 0.5×0.5 mm, whereas the stress concentration region is only about 0.1×0.1 mm.

In conclusion, FAST is a useful tool for providing qualitative experimental validation of the overall stress field in a component provided it is suitably constrained and loaded but FAST does not detect localised stress concentrations.

5. Conclusions and Recommendations

A preliminary finite element stress analysis of the fourth stage low pressure compressor disc of the TF30 engine has been completed and the following conclusions can be made.

1. The interference fit between the spacer and the snap on the front side of the disc, which was simulated in this model by a pressure load, does not affect the stress range for major engine usage cycles but does increase the mean and peak stresses.
2. The thermal stresses are very small, as expected because the temperatures and temperature gradients are not very high.
3. The stresses in the snap fillet radius caused by the rotation of the disc are more than twice as large as the stresses caused by the assembly load resulting from the interference fit between the disc and the spacer.
4. The predicted stresses are well below the yield stress and further work using a more sophisticated model is recommended to determine whether the design of the disc is really this conservative.
5. Axial fatigue tests validated the FEA predicted failure location.
6. FAST can provide useful experimental data for qualitative validation of FEA results.

The following recommendations for further work are made:

1. A two-dimensional axisymmetric model of the fourth stage disc including the spacers which are bolted to the disc, the tie rod sleeves and the fourth stage air seal should be created. This model should use contact surfaces to model the interactions between the components and the loads created by the interference fits between the spacers and the front and rear snaps on the disc. It should also include a refined mesh - particularly around the snap fillet radius region.
2. A two-dimensional axisymmetric model of the complete TF30 fan/LPC assembly to identify the loads and boundary conditions for the fourth stage disc more accurately should be created.
3. A three-dimensional model of the fourth stage disc and spacers to determine the effect of the non-axisymmetric features should be created.
4. The sensitivity of the peak stress to the snap radius dimension should be investigated and compared to the promulgated life data from PWA.
5. The variation of material properties as a function of temperature should be incorporated in the model.

6. Acknowledgments

The following people have all contributed to this work:

Simon McLean, Neil Swansson, Gordon Stocks, Jianfu Hou, Manfred Heller, Wyman Zhuang, Tom Ryall, David Rowlands, Tom Radtke, Bryon Wicks, Steve Sanderson, Julian Paul, Boeing drawing office, George Millers, 501 Wing, DTA

7. References

1. PARKS, R., *Report on TF30 Engine Component Retirement for Cause (RFC) Study*, September 1997
2. HARRIS, J., *Engine component retirement for cause*, AFMAL-TR-87-4069, 1987.
3. PRATT & WHITNEY AIRCRAFT TF 30 Air Force Engines-LCF Life Assessment, June 30, 1983
4. PRATT & WHITNEY AIRCRAFT, Drawing Number 77445H559504 dated 14 August 1968
5. SMITH, W.F. AND VALCICH, P.J., *TF30-P-3 Temperature Survey Test*, FR-10333, Pratt & Whitney Aircraft Group, December 1978.
6. ROARK, R.J. AND YOUNG, W.C., *Formulas for Stress and Strain*, 5th Ed., McGraw Hill 1975.
7. RYALL T.G. AND WONG A.K., "The design of a focal-plane array thermographic stress analysis system", Exp. Mech, 1995, pp144-147.
8. NAFEMS, *A Finite Element Primer*, Published by NAFEMS, Glasgow, October 1986

Table 1. Load cases.

| Case No. | Centrifugal Load | Interference Load [psi] | Temperature Field |
|----------|------------------|-------------------------|-------------------|
| 1 | - | 450 | - |
| 2 | - | 900 | - |
| 3 | IDLE | - | - |
| 4 | MIL | - | - |
| 5 | - | - | IDLE |
| 6 | - | - | MIL |
| 7 | IDLE | 450 | IDLE |
| 8 | IDLE | 900 | IDLE |
| 9 | MIL | 450 | MIL |
| 10 | MIL | 900 | MIL |

Table 2. Disc temperatures at IDLE and MIL power.

| Location | IDLE Temperature [°F] | MIL Temperature [°F] |
|-----------|-----------------------|----------------------|
| Bore | 146 | 416 |
| Inner Web | 129 | 381 |
| Rim | 109 | 288 |

Table 3. Stress results at selected locations on the disc for load cases 1 to 4.

| Location | Node ID | σ_{xx} (ksi) | σ_{yy} (ksi) | σ_{zz} (ksi) | σ_1 (ksi) | σ_2 (ksi) | σ_3 (ksi) |
|-----------------|---------|---------------------|---------------------|---------------------|------------------|------------------|------------------|
| Case 1 | | | | | | | |
| Bore | 2732 | 0.0 | 0.1 | -0.8 | 0.1 | 0.0 | -0.8 |
| Inner Web Rear | 3192 | -0.3 | 0.0 | -0.6 | 0.0 | -0.3 | -0.6 |
| Inner Web Front | 3210 | -0.3 | -0.1 | -1.3 | 0.0 | -0.4 | -1.3 |
| Snap | 3750 | 8.2 | 5.2 | 3.4 | 11.6 | 3.4 | 1.8 |
| Snap | 3777 | 9.7 | 3.2 | 3.3 | 11.3 | 3.3 | 1.7 |
| Snap | 3793 | 9.5 | 2.1 | 2.8 | 10.3 | 2.8 | 1.2 |
| Snap | 3804 | 9.1 | 1.6 | 2.5 | 9.5 | 2.5 | 1.2 |
| Rim | 4609 | 0.0 | 0.0 | -0.5 | 0.0 | 0.0 | -0.5 |
| Outer Web Front | 8283 | 0.1 | 0.0 | -0.4 | 0.1 | 0.0 | -0.4 |
| Case 2 | | | | | | | |
| Bore | 2732 | 0.0 | 0.1 | -1.6 | 0.1 | 0.0 | -1.6 |
| Inner Web Rear | 3192 | -0.7 | 0.0 | -1.2 | 0.0 | -0.7 | -1.2 |
| Inner Web Front | 3210 | -0.5 | -0.2 | -2.6 | 0.1 | -0.8 | -2.6 |
| Snap | 3750 | 16.4 | 10.3 | 6.8 | 23.3 | 6.8 | 3.5 |
| Snap | 3777 | 19.5 | 6.5 | 6.6 | 22.6 | 6.6 | 3.3 |
| Snap | 3793 | 18.9 | 4.1 | 5.6 | 20.7 | 5.6 | 2.4 |
| Snap | 3804 | 18.1 | 3.3 | 5.1 | 18.9 | 5.1 | 2.5 |
| Rim | 4609 | 0.0 | 0.0 | -1.0 | 0.0 | 0.0 | -1.0 |
| Outer Web Front | 8283 | 0.1 | 0.0 | -0.9 | 0.1 | 0.0 | -0.9 |
| Case 3 | | | | | | | |
| Bore | 2732 | 0.0 | -0.7 | 12.0 | 12.0 | 0.0 | -0.7 |
| Inner Web Rear | 3192 | 12.9 | 0.0 | 14.2 | 14.2 | 12.9 | 0.0 |
| Inner Web Front | 3210 | -1.6 | -0.9 | 9.1 | 9.1 | -0.1 | -2.5 |
| Snap | 3750 | 5.7 | 2.3 | 12.2 | 12.2 | 7.2 | 0.7 |
| Snap | 3777 | 9.0 | 2.3 | 13.3 | 13.3 | 9.9 | 1.4 |
| Snap | 3793 | 9.7 | 1.7 | 13.3 | 13.3 | 10.2 | 1.2 |
| Snap | 3804 | 10.1 | 1.7 | 13.4 | 13.4 | 10.4 | 1.4 |
| Rim | 4609 | 1.3 | 0.1 | 6.9 | 6.9 | 1.3 | 0.1 |
| Outer Web Front | 8283 | 14.1 | 0.5 | 13.3 | 14.1 | 13.3 | 0.4 |
| Case 4 | | | | | | | |
| Bore | 2732 | -0.1 | -2.7 | 48.1 | 48.1 | -0.1 | -2.7 |
| Inner Web Rear | 3192 | 51.5 | 0.1 | 56.9 | 56.9 | 51.5 | 0.1 |
| Inner Web Front | 3210 | -6.5 | -3.6 | 36.2 | 36.2 | -0.3 | -9.9 |
| Snap | 3750 | 22.9 | 9.0 | 48.6 | 48.6 | 29.0 | 3.0 |
| Snap | 3777 | 36.0 | 9.2 | 53.0 | 53.0 | 39.6 | 5.6 |
| Snap | 3793 | 38.8 | 6.9 | 53.2 | 53.2 | 40.9 | 4.8 |
| Snap | 3804 | 40.5 | 6.7 | 53.7 | 53.7 | 41.5 | 5.6 |
| Rim | 4609 | 5.0 | 0.4 | 27.4 | 27.4 | 5.0 | 0.4 |
| Outer Web Front | 8283 | 56.3 | 1.8 | 53.1 | 56.6 | 53.1 | 1.5 |

Table 4. Stress results at selected locations on the disc for load cases 5 to 8.

| Location | Node ID | σ_{xx} (ksi) | σ_{yy} (ksi) | σ_{zz} (ksi) | σ_1 (ksi) | σ_2 (ksi) | σ_3 (ksi) |
|-----------------|---------|---------------------|---------------------|---------------------|------------------|------------------|------------------|
| Case 5 | | | | | | | |
| Bore | 2732 | 0.0 | 0.1 | -1.5 | 0.1 | 0.0 | -1.5 |
| Inner Web Rear | 3192 | -1.3 | 0.0 | -0.2 | 0.0 | -0.2 | -1.3 |
| Inner Web Front | 3210 | 0.2 | 0.1 | 0.3 | 0.3 | 0.2 | 0.0 |
| Snap | 3750 | -0.2 | 0.0 | 0.3 | 0.3 | 0.0 | -0.2 |
| Snap | 3777 | -0.4 | -0.1 | 0.2 | 0.2 | 0.0 | -0.4 |
| Snap | 3793 | -0.5 | -0.1 | 0.2 | 0.2 | -0.1 | -0.5 |
| Snap | 3804 | -0.5 | -0.1 | 0.1 | 0.1 | -0.1 | -0.5 |
| Rim | 4609 | 0.0 | 0.0 | 1.4 | 1.4 | 0.0 | 0.0 |
| Outer Web Front | 8283 | -0.6 | 0.0 | 0.8 | 0.8 | 0.0 | -0.6 |
| Case 6 | | | | | | | |
| Bore | 2732 | 0.0 | 0.3 | -4.5 | 0.3 | 0.0 | -4.5 |
| Inner Web Rear | 3192 | -4.6 | 0.0 | -1.8 | 0.0 | -1.8 | -4.6 |
| Inner Web Front | 3210 | 0.6 | 0.3 | -0.1 | 0.9 | 0.0 | -0.1 |
| Snap | 3750 | -1.0 | -0.2 | -0.1 | 0.0 | -0.1 | -1.1 |
| Snap | 3777 | -1.9 | -0.4 | -0.4 | -0.3 | -0.4 | -2.0 |
| Snap | 3793 | -2.1 | -0.3 | -0.5 | -0.2 | -0.5 | -2.2 |
| Snap | 3804 | -2.3 | -0.4 | -0.5 | -0.3 | -0.5 | -2.3 |
| Rim | 4609 | 0.0 | 0.0 | 5.6 | 5.6 | 0.0 | 0.0 |
| Outer Web Front | 8283 | -2.4 | -0.1 | 2.8 | 2.8 | -0.1 | -2.4 |
| Case 7 | | | | | | | |
| Bore | 2732 | 0.0 | -0.5 | 9.8 | 9.8 | 0.0 | -0.5 |
| Inner Web Rear | 3192 | 11.2 | 0.0 | 13.4 | 13.4 | 11.2 | 0.0 |
| Inner Web Front | 3210 | -1.7 | -0.9 | 8.0 | 8.0 | 0.0 | -2.6 |
| Snap | 3750 | 13.8 | 7.4 | 15.8 | 18.7 | 15.8 | 2.6 |
| Snap | 3777 | 18.4 | 5.5 | 16.7 | 20.8 | 16.7 | 3.0 |
| Snap | 3793 | 18.7 | 3.7 | 16.3 | 20.1 | 16.3 | 2.4 |
| Snap | 3804 | 18.7 | 3.2 | 16.1 | 19.3 | 16.1 | 2.6 |
| Rim | 4609 | 1.2 | 0.1 | 7.7 | 7.7 | 1.3 | 0.1 |
| Outer Web Front | 8283 | 13.5 | 0.4 | 13.6 | 13.6 | 13.6 | 0.4 |
| Case 8 | | | | | | | |
| Bore | 2732 | 0.0 | -0.5 | 9.0 | 9.0 | 0.0 | -0.5 |
| Inner Web Rear | 3192 | 10.9 | 0.0 | 12.8 | 12.8 | 10.9 | 0.0 |
| Inner Web Front | 3210 | -2.0 | -1.1 | 6.8 | 6.8 | 0.0 | -3.1 |
| Snap | 3750 | 22.0 | 12.6 | 19.2 | 30.3 | 19.2 | 4.3 |
| Snap | 3777 | 28.1 | 8.7 | 20.0 | 32.1 | 20.0 | 4.7 |
| Snap | 3793 | 28.2 | 5.8 | 19.1 | 30.4 | 19.1 | 3.6 |
| Snap | 3804 | 27.7 | 4.9 | 18.6 | 28.8 | 18.6 | 3.8 |
| Rim | 4609 | 1.3 | 0.1 | 7.2 | 7.2 | 1.3 | 0.1 |
| Outer Web Front | 8283 | 13.6 | 0.4 | 13.1 | 13.7 | 13.1 | 0.4 |

Table 5. Stress results at selected locations on the disc for load cases 9 and 10.

| Location | Node ID | σ_{xx} (ksi) | σ_{yy} (ksi) | σ_{zz} (ksi) | σ_1 (ksi) | σ_2 (ksi) | σ_3 (ksi) |
|-----------------|---------|---------------------|---------------------|---------------------|------------------|------------------|------------------|
| Case 9 | | | | | | | |
| Bore | 2732 | -0.1 | -2.4 | 42.8 | 42.8 | -0.1 | -2.4 |
| Inner Web Rear | 3192 | 46.6 | 0.1 | 54.4 | 54.4 | 46.6 | 0.1 |
| Inner Web Front | 3210 | -6.2 | -3.4 | 34.9 | 34.9 | -0.2 | -9.4 |
| Snap | 3750 | 30.2 | 14.0 | 52.0 | 52.0 | 39.4 | 4.8 |
| Snap | 3777 | 43.9 | 12.0 | 55.9 | 55.9 | 48.9 | 7.0 |
| Snap | 3793 | 46.2 | 8.6 | 55.5 | 55.5 | 49.0 | 5.7 |
| Snap | 3804 | 47.2 | 8.0 | 55.7 | 55.7 | 48.6 | 6.6 |
| Rim | 4609 | 5.0 | 0.4 | 32.5 | 32.5 | 5.0 | 0.4 |
| Outer Web Front | 8283 | 53.9 | 1.8 | 55.4 | 55.4 | 54.2 | 1.5 |
| Case 10 | | | | | | | |
| Bore | 2732 | -0.1 | -2.4 | 42.0 | 42.0 | -0.1 | -2.4 |
| Inner Web Rear | 3192 | 46.3 | 0.1 | 53.8 | 53.8 | 46.3 | 0.1 |
| Inner Web Front | 3210 | -6.5 | -3.6 | 33.6 | 33.6 | -0.2 | -9.8 |
| Snap | 3750 | 38.4 | 19.2 | 55.4 | 55.4 | 51.0 | 6.6 |
| Snap | 3777 | 53.6 | 15.3 | 59.2 | 60.2 | 59.2 | 8.7 |
| Snap | 3793 | 55.6 | 10.7 | 58.3 | 59.4 | 58.3 | 7.0 |
| Snap | 3804 | 56.3 | 9.6 | 58.2 | 58.2 | 58.1 | 7.8 |
| Rim | 4609 | 5.0 | 0.4 | 32.0 | 32.0 | 5.0 | 0.4 |
| Outer Web Front | 8283 | 54.0 | 1.8 | 55.0 | 55.0 | 54.3 | 1.5 |

Table 6. Summary of stress results at snap fillet radius for an operating engine.

| Case No. | Centrifugal Load | Interference Load [psi] | Temperature Field | Max. Principal Stress [ksi] |
|----------|------------------|-------------------------|-------------------|-----------------------------|
| 7 | IDLE | 450 | IDLE | 20.8 |
| 8 | IDLE | 900 | IDLE | 32.1 |
| 9 | MIL | 450 | MIL | 55.9 |
| 10 | MIL | 900 | MIL | 60.2 |

Table 7. Stress range at node 3777 for combined loads for major engine usage cycles.

| Cycle Type | Stress range in x-y plane parallel to free surface (ksi) | Stress range in z direction (ksi) |
|------------|--|-----------------------------------|
| IDLE-MIL | 28.1 | 39.2 |
| STOP-MIL | 37.6 | 52.6 |

Table 8: Summary of axial fatigue tests on coupon specimens cut directly from the 4th LPC

| Test number | σ_{max} | σ_{mean} | σ_{min} | frequency | Nf |
|-------------|----------------|-----------------|----------------|-----------|-----------|
| 1 | 440 | 268 | 32 | 5Hz | 154,079 |
| 2 | 363 | 199 | 34 | 5Hz | 117,898 |
| 3 | 321 | 176 | 30 | 5Hz | 1,007,651 |

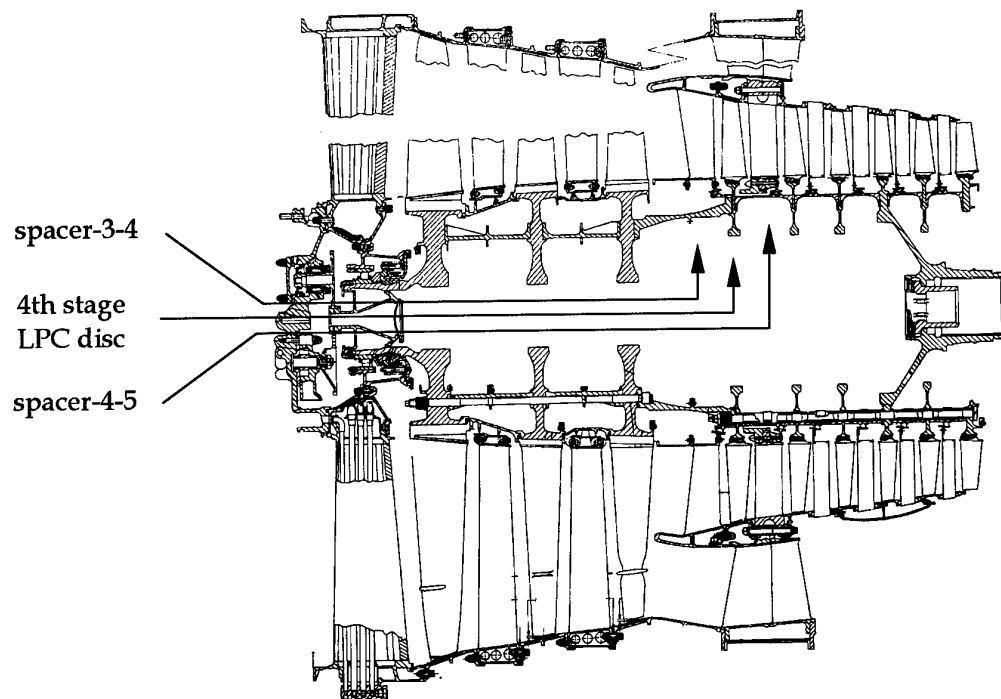


Figure 1. Cross-section of TF30 fan & LPC.

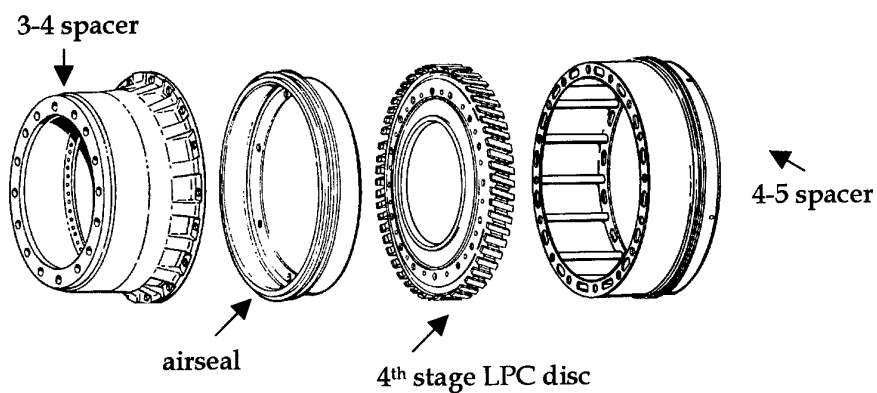


Figure 2. Exploded view of fourth LPC disc assembly.

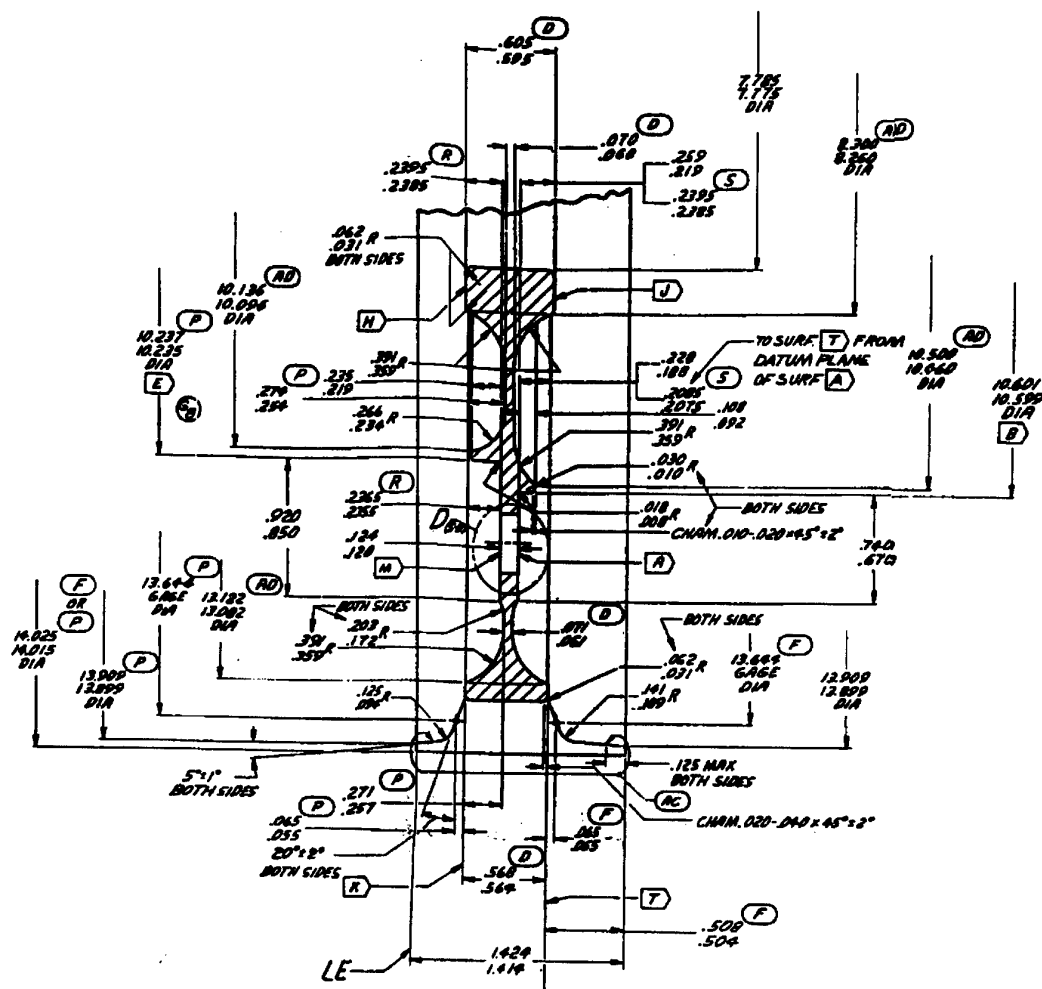


Figure 3. Geometry of cross-section of disc.

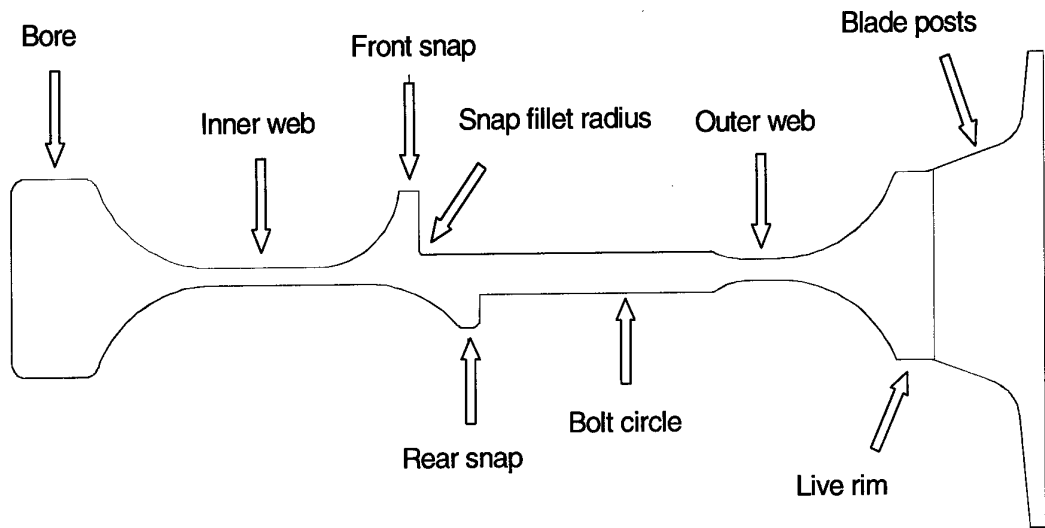


Figure 4. Schematic of cross-section of disc.

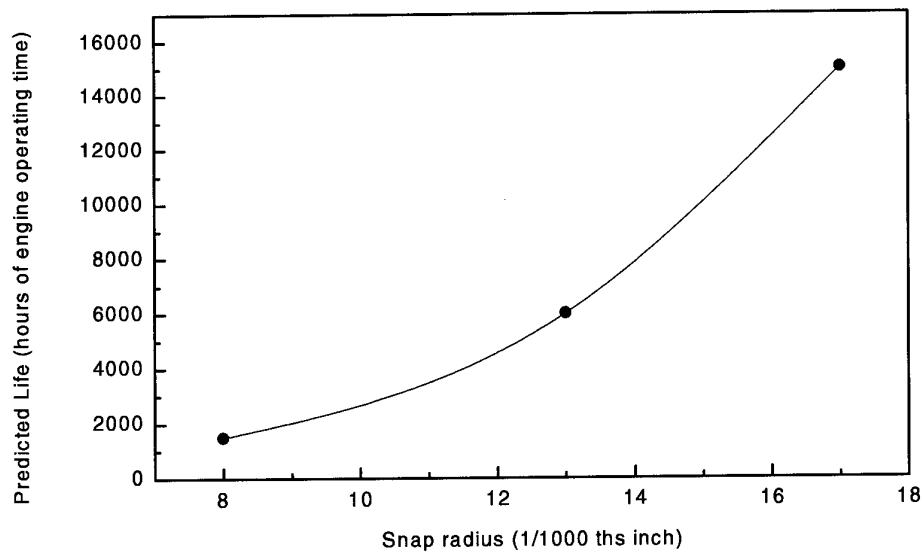


Figure 5. Disc retirement life as a function of the snap fillet radius [3].

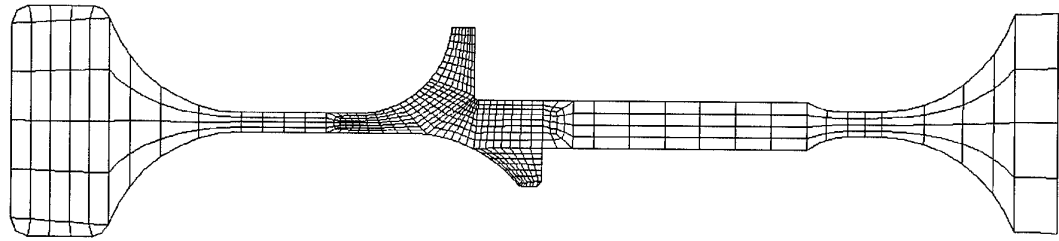


Figure 6. The complete mesh.

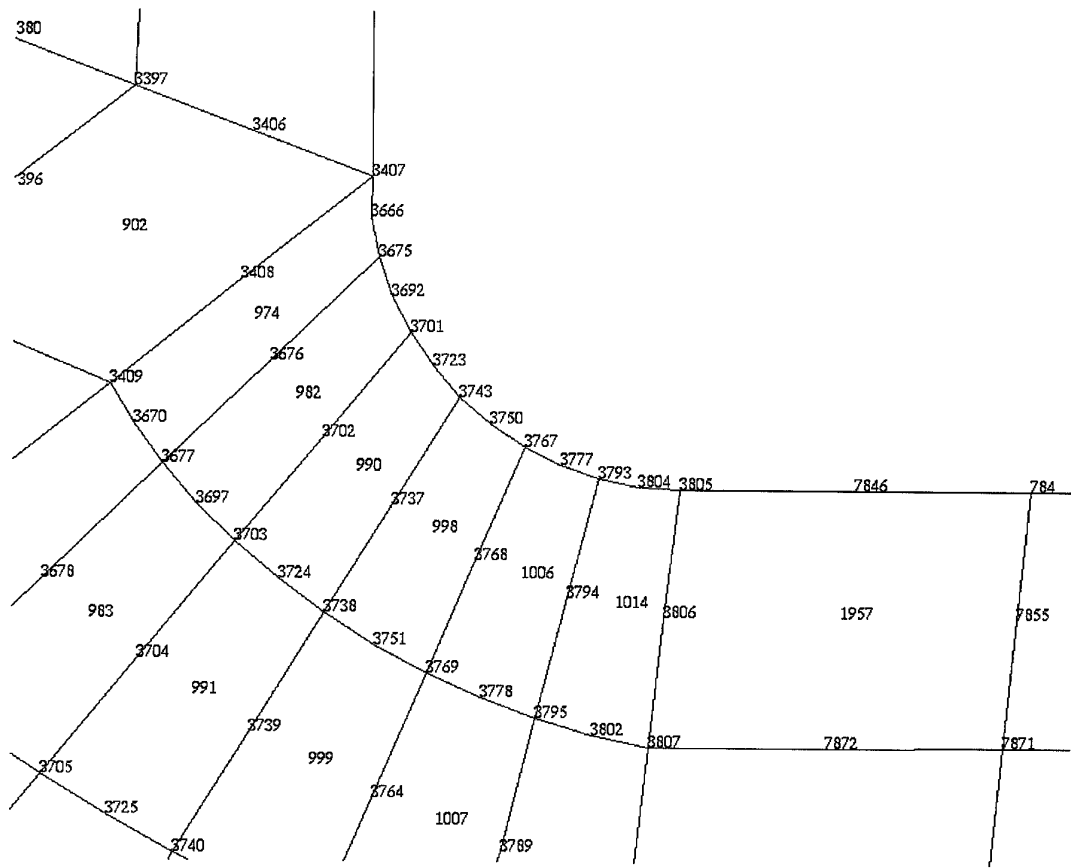


Figure 7. Six elements around snap fillet radius showing node and element numbers.

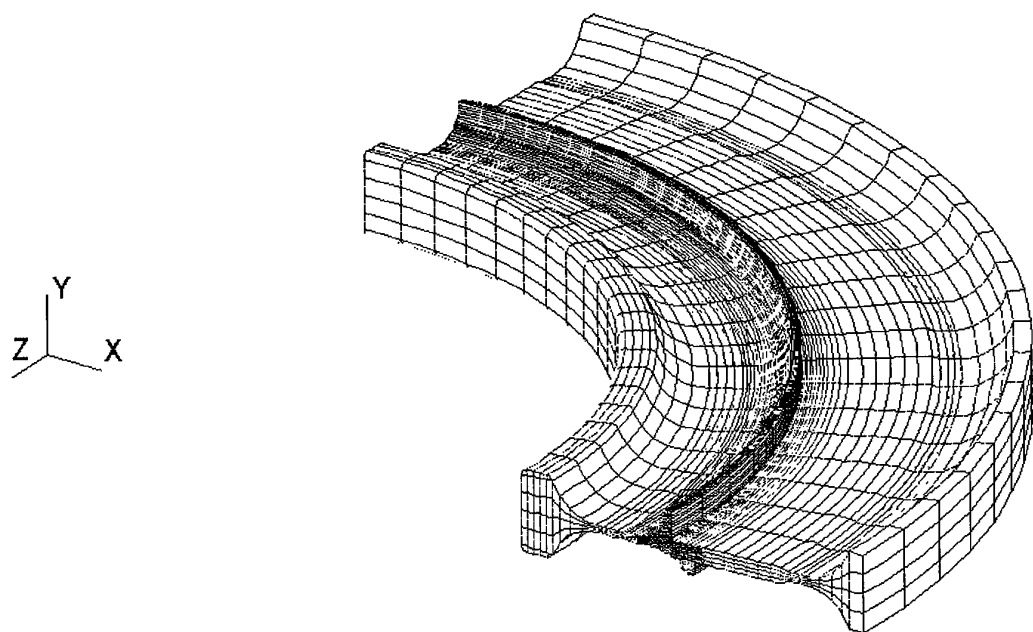


Figure 8. Swept mesh for visualization purposes only.

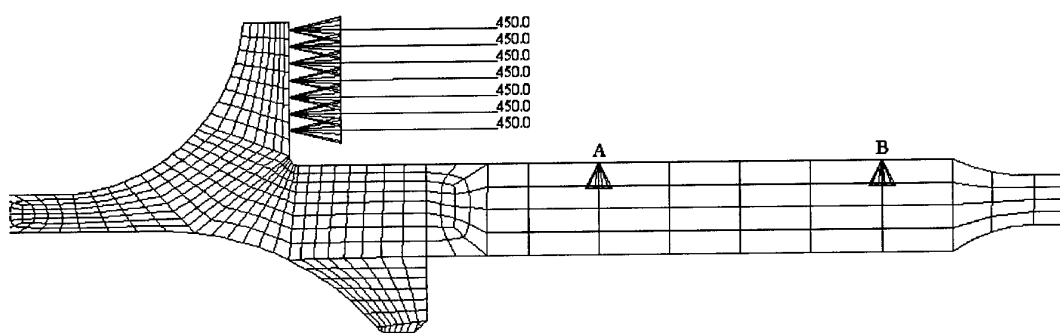


Figure 9. The constraints in the y-direction at points A and B at the bolt circle, and the load of 450 psi on the front snap.

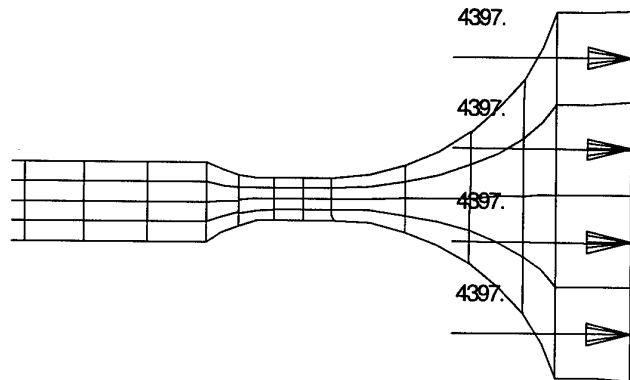


Figure 10. Simulated blade load of 4397 psi at MIL power.

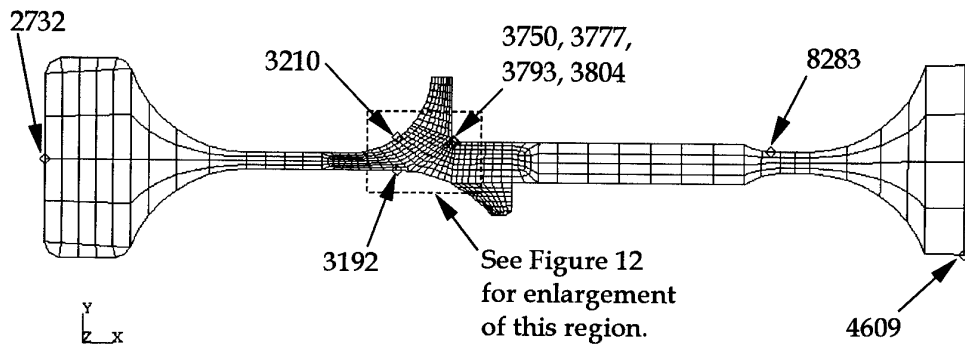


Figure 11. Nodes for which results are presented.

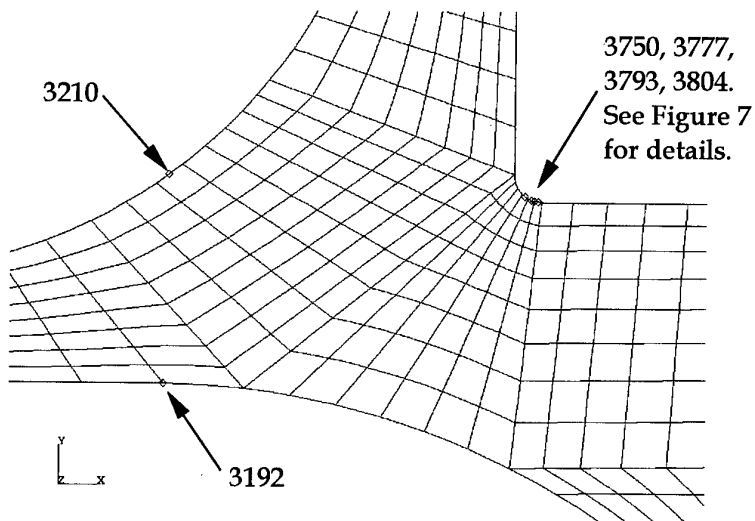


Figure 12. Detail of nodes for which results are presented.

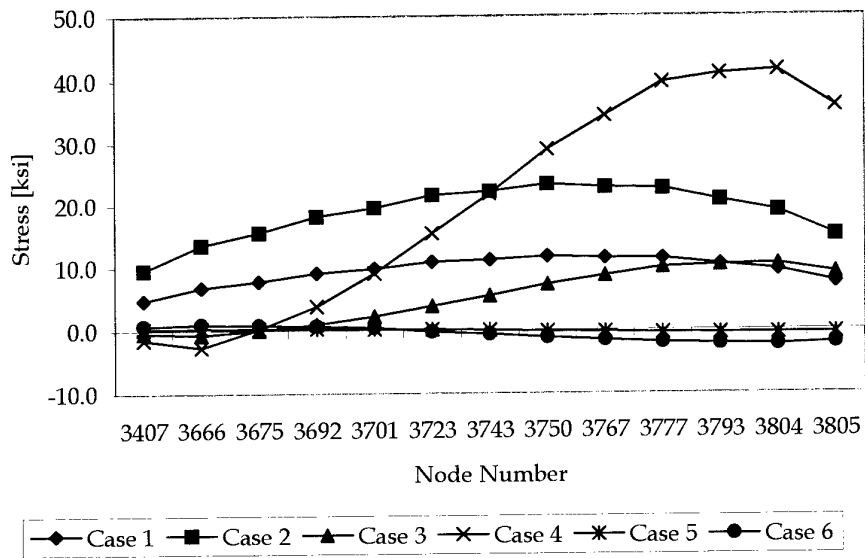


Figure 13. Principal stress at snap parallel to free surface in X-Y plane.

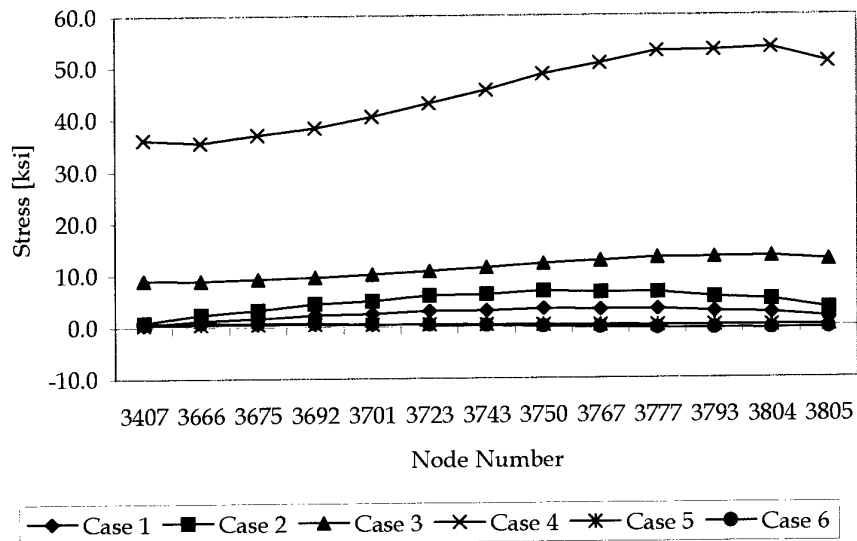


Figure 14. Principal stress at snap in Z direction (hoop).

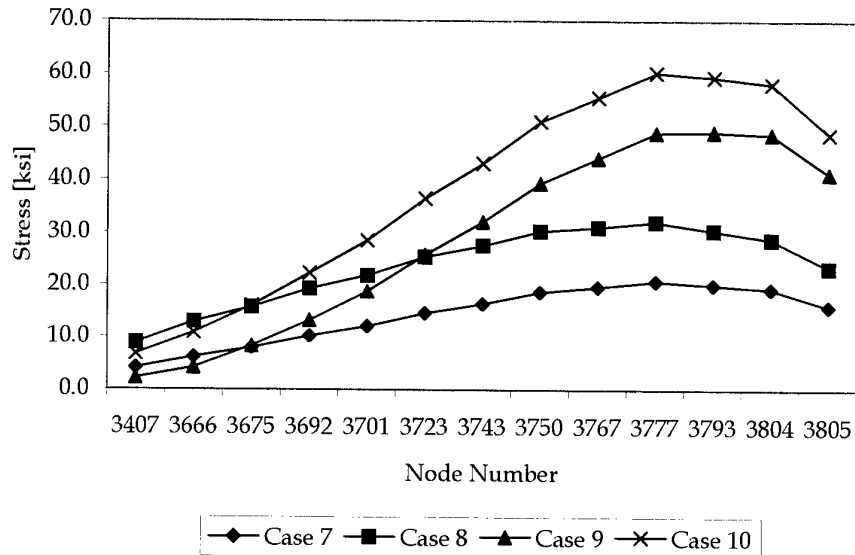


Figure 15. Principal stress at snap parallel to free surface in X-Y plane.

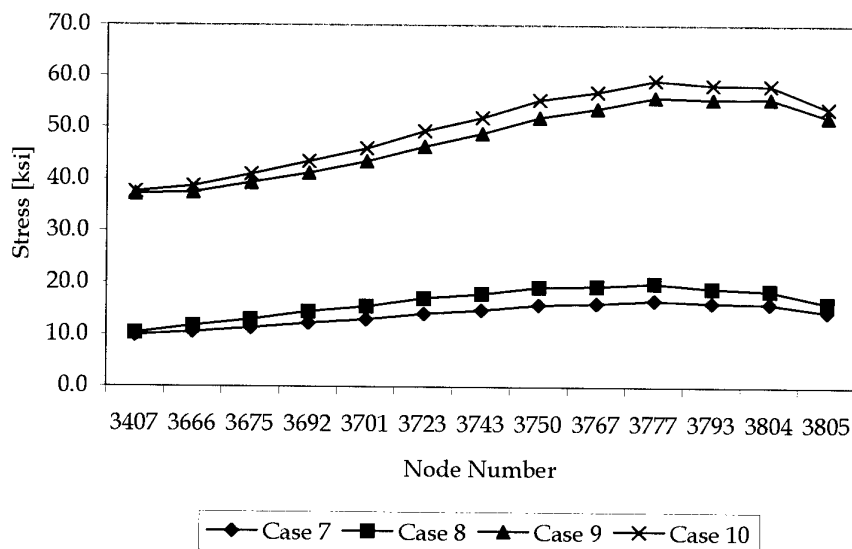


Figure 16. Principal stress at snap in Z direction (hoop).

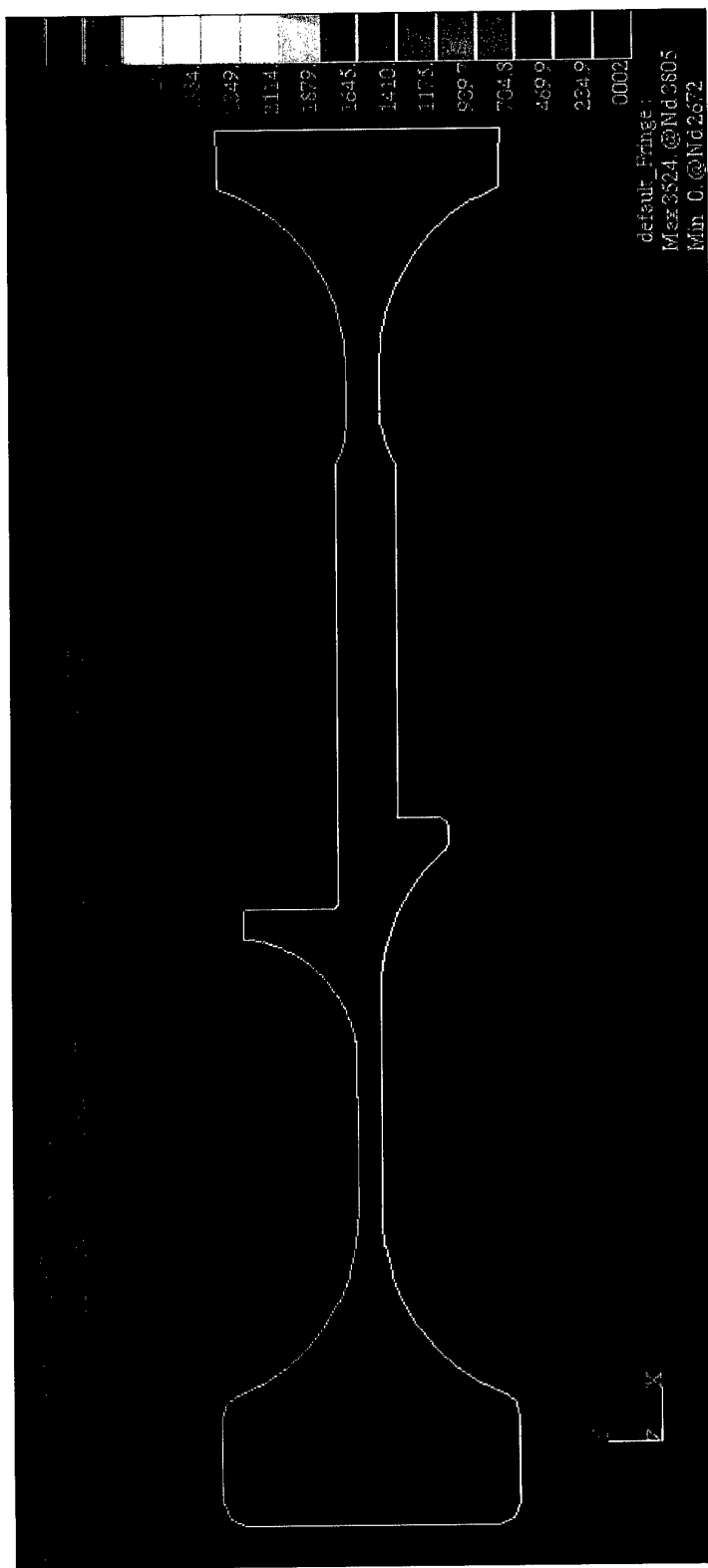


Figure 17. The stress difference plot for load case 2 (psi).

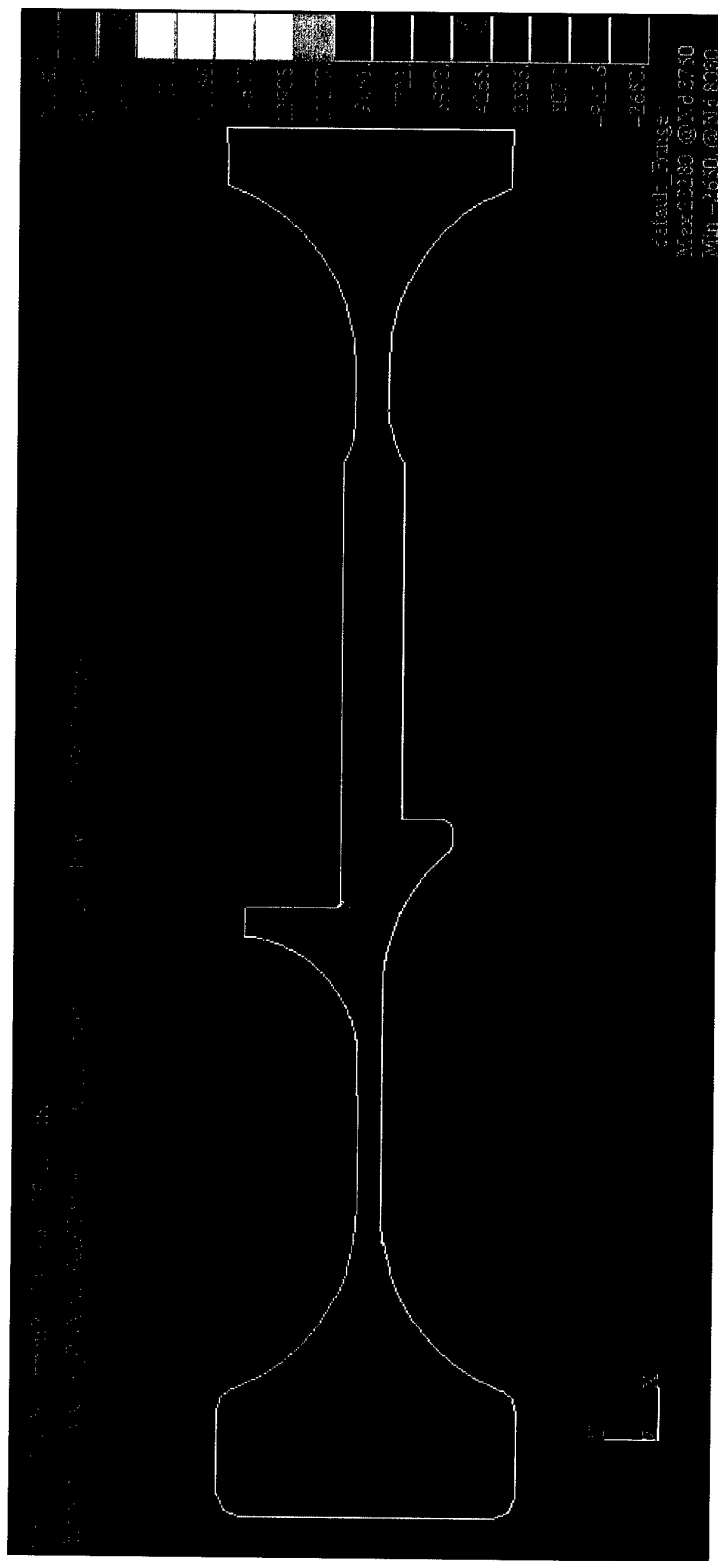


Figure 18. The maximum principal stress contours for load case 2 (psi).

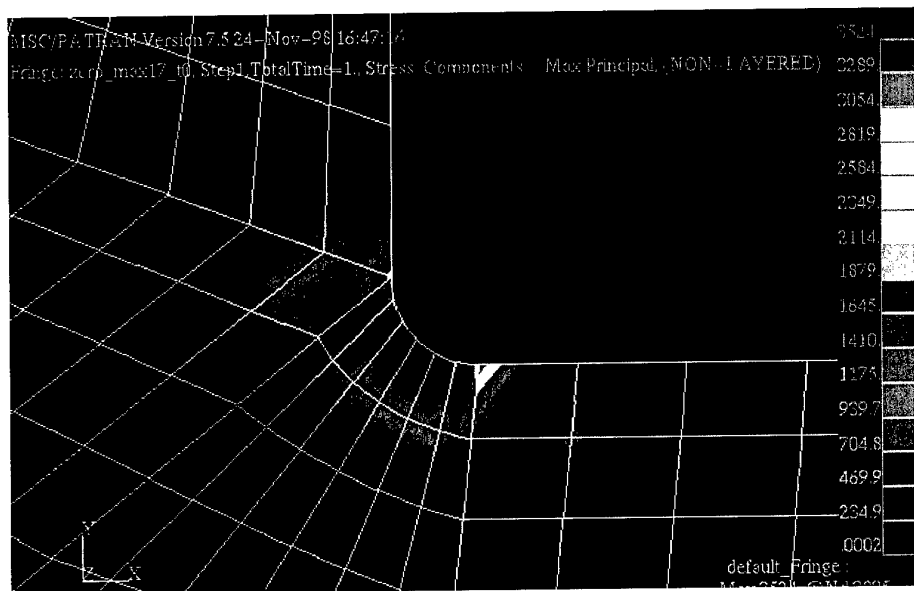


Figure 19. Detail of the stress difference plot for load case 2 for the snap region (psi).

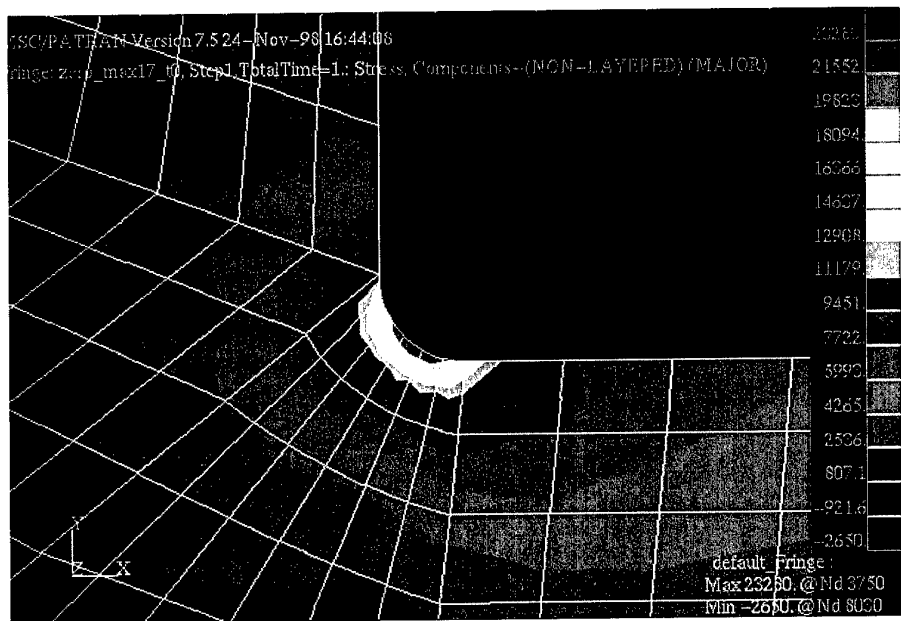
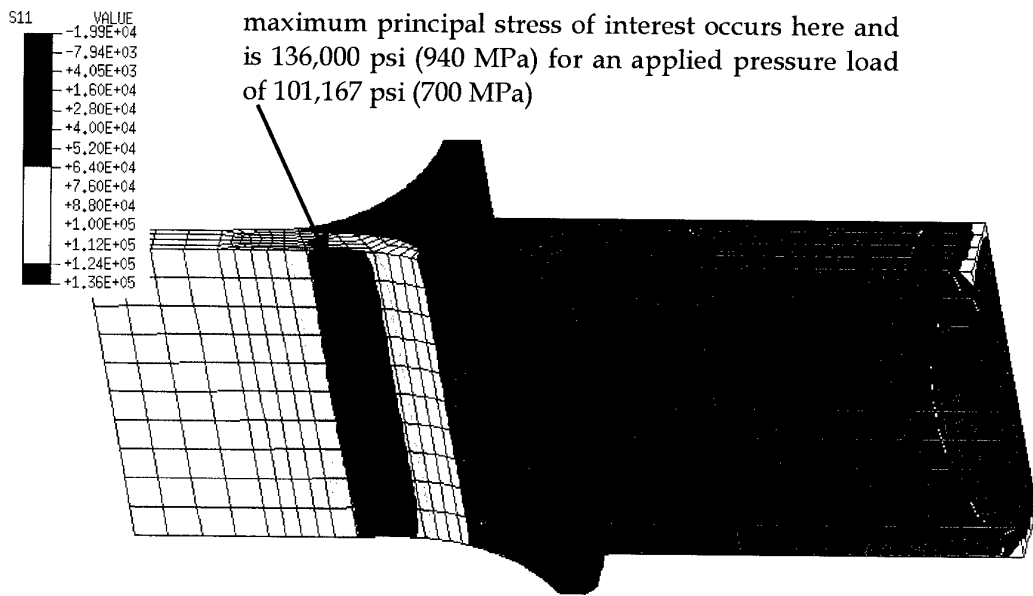
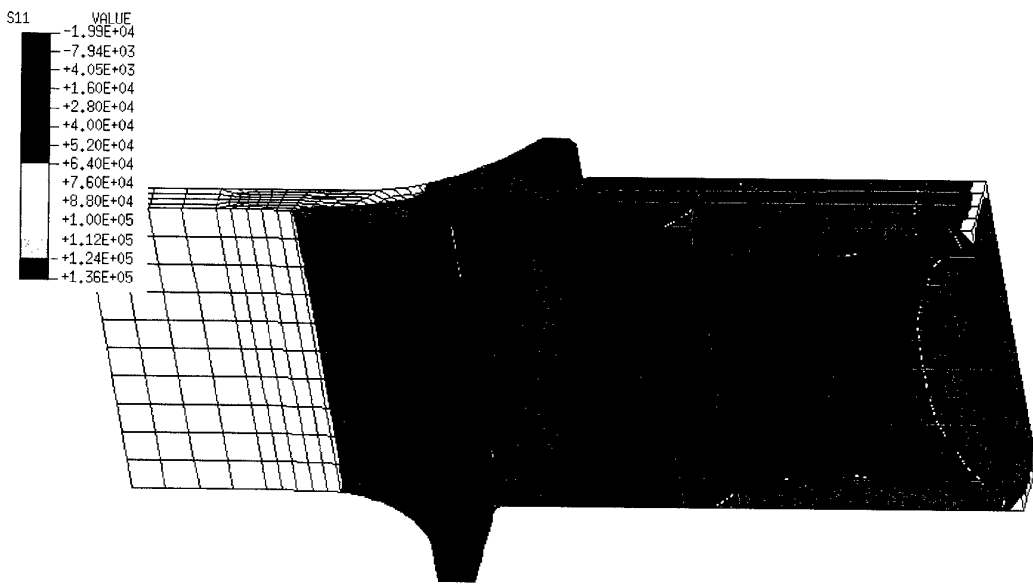


Figure 20. Detail of the maximum principal stress contour plot for load case 2 for the snap region (psi).



(a) Aft view



(b) Forward view

Figure 21. Stress results from 3D finite element model of test specimen in tension .

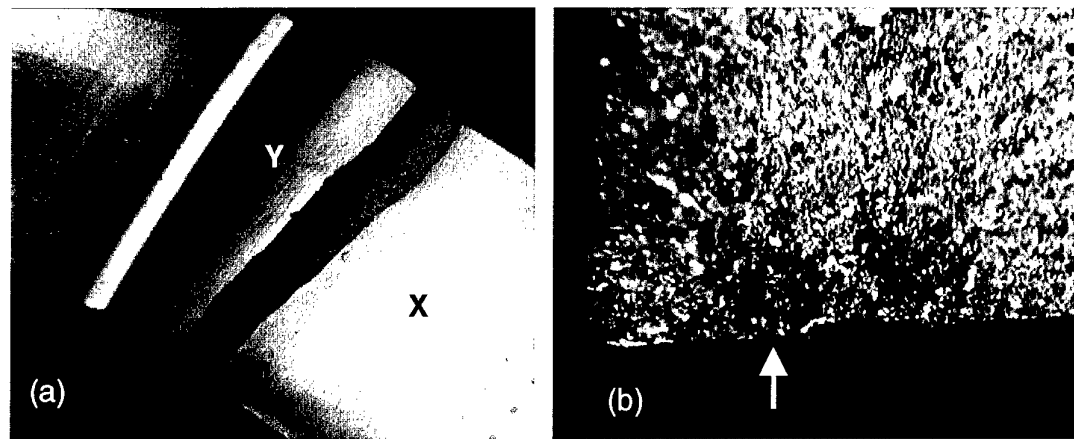


Figure 22 (a) Fatigue crack origin on inner web (X) adjacent to front snap runout radius (Y) (refer fig 3),
(b) detail of the fracture surface of (a) showing the fatigue origin, arrowed.

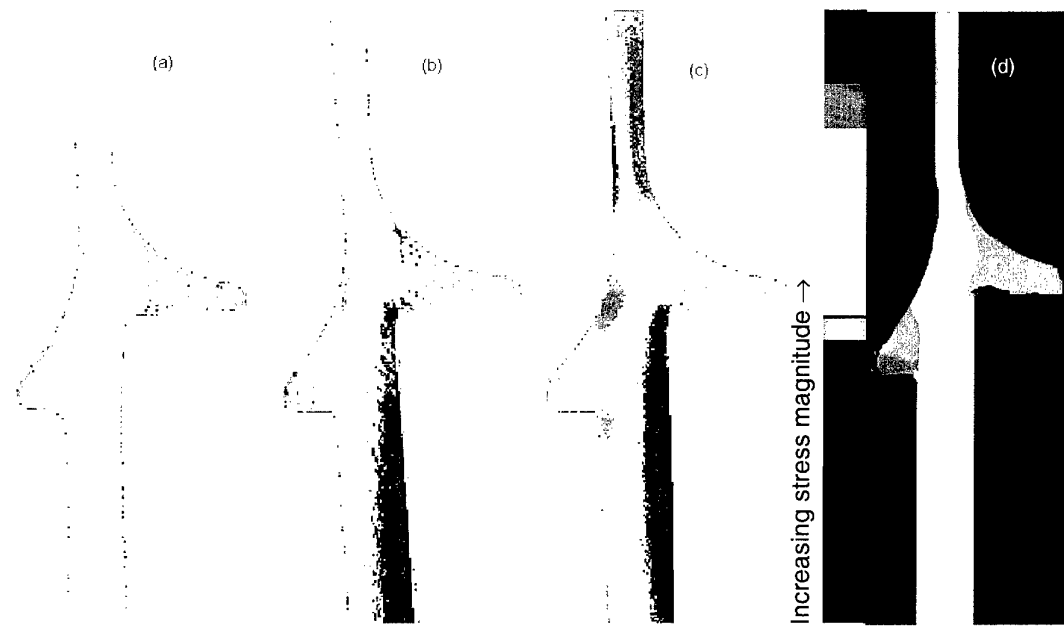


Figure 23. FAST side view of TF 30 4th stage LPC with alternating compressive loading,
(a) no interference (b) small interference and (c) large interference.
(d) FEA results for 1st stress invariant.

DSTO-TR-0915

Appendix 1

Benchmark Examples

As a first step in the finite element analysis of the compressor disc some simple benchmark cases of rotating discs were modelled to ensure the correct results were obtained.

Benchmark Example 1 - an annular disc of uniform thickness.

The disc has an outer radius of $R = 10.0''$, with a central hole of radius $R_0 = 2.0''$, and a uniform thickness of $2.0''$ (Fig. A1). The disc rotates about its own axis with a uniform angular velocity of $\omega = 377.0 \text{ rad/s}$ (3600 rpm).

The finite element mesh consisted of 8-node biquadratic axisymmetric solid elements. There were 40 elements in the radial direction and 6 elements through the thickness of the disc (Fig. A1).

Typical material properties for steel were used:

Young's Modulus = 30,000,000 psi

Poisson's ratio $\nu = 0.3$

Density (in units for theoretical calculation) $\delta = 0.279 \text{ lbm/in}^3$

Density (in units for FEA) $\rho = 0.0007226 \text{ lbf s}^2/\text{in}^4$

The theoretical formulae for the stresses in a homogenous annular disc of uniform thickness rotating about its own axis with a uniform angular velocity are given by Roark & Young [6].

The radial stress as a function of the distance r from the central axis is given by

$$\sigma_r = \frac{3+\nu}{8} \frac{\delta\omega^2}{386.4} \left(R^2 + R_0^2 - \frac{R^2 R_0^2}{r^2} - r^2 \right) \text{lb/in}^2 \quad (\text{A.1})$$

The tangential or hoop stress as a function of the distance r from the central axis is given by

$$\sigma_t = \frac{1}{8} \frac{\delta\omega^2}{386.4} \left[(3+\nu) \left(R^2 + R_0^2 + \frac{R^2 R_0^2}{r^2} \right) - (1+3\nu)r^2 \right] \text{lb/in}^2 \quad (\text{A.2})$$

The results calculated using the theoretical formulae are plotted in Figure A2 on the same axes as the results of the finite element analysis. There is so little difference between the two sets of results that it is hard to distinguish the separate curves which lie on top of each other.

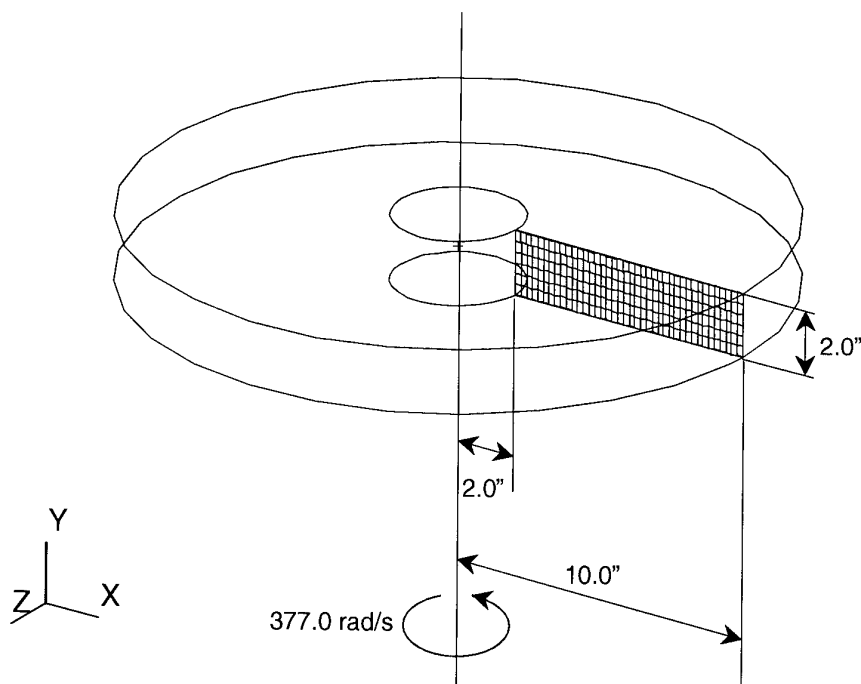


Figure A1. The geometry and mesh for the disc with uniform thickness.

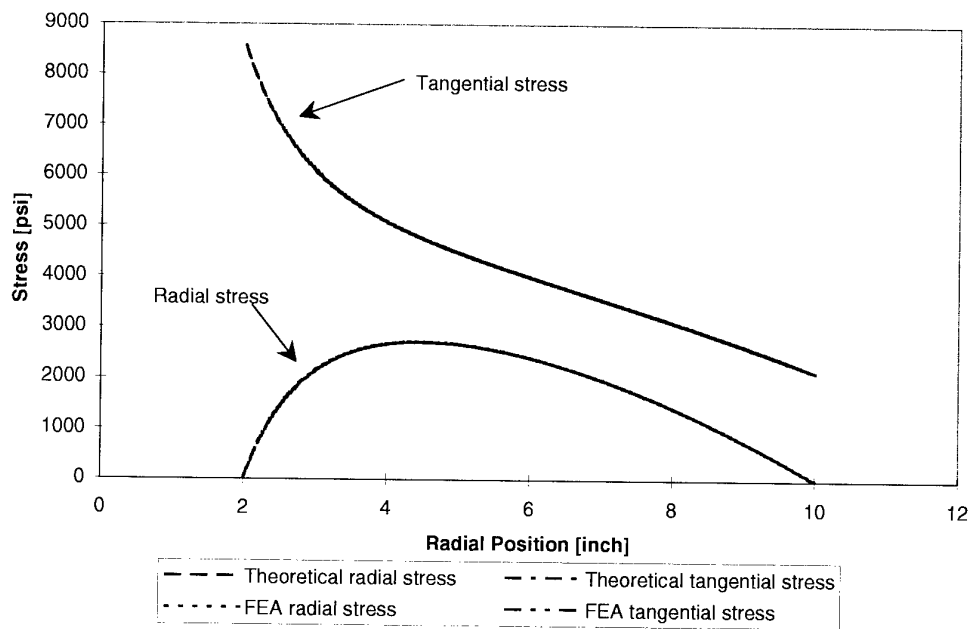


Figure A2. Comparison of theoretical and FEA stress results for the rotating annular disc with uniform thickness.

Benchmark Example 2 - an annular disc with hyperbolic thickness.

The disc has an outer radius of $R = 10.0''$, with a central hole of radius $R_0 = 2.0''$, and a hyperbolic thickness profile varying from $3.0''$ at the bore to $1.0''$ at the rim. (Fig. A2). The thickness of the disc is defined by the equation

$$t = cr^a \quad (\text{A.3})$$

where t is the thickness at radius r , $c = 4.819$, $a = -0.6826$.

The disc rotates about its own axis with a uniform angular velocity of $\omega = 377.0 \text{ rad/s}$ (3600 rpm).

The finite element mesh consisted of 8-node biquadratic axisymmetric solid elements. There were 40 elements in the radial direction and 6 elements through the thickness of the disc (Fig. A2).

Typical material properties for steel were used:

Young's Modulus = 30,000,000 psi

Poisson's ratio $\nu = 0.3$

Density (in units for theoretical calculation) $\delta = 0.279 \text{ lbm/in}^3$

Density (in units for FEA) $\rho = 0.0007226 \text{ lbf s}^2/\text{in}^4$

The theoretical formulae for the stresses in a homogenous annular disc with hyperbolic thickness rotating about its own axis with a uniform angular velocity are given by Roark & Young [6].

The radial stress as a function of the distance r from the central axis is given by

$$\sigma_r = \frac{E}{1-\nu^2} [(3+\nu)Fr^2 + (m_1+\nu)Ar^{m_1-1} + (m_2+\nu)Br^{m_2-1}] \text{lb/in}^2 \quad (\text{A.4})$$

The tangential or hoop stress as a function of the distance r from the central axis is given by

$$\sigma_r = \frac{E}{1-\nu^2} [(1+3\nu)Fr^2 + (1+m_1\nu)Ar^{m_1-1} + (1+m_2\nu)Br^{m_2-1}] \text{lb/in}^2 \quad (\text{A.5})$$

where

$$F = \frac{-(1-\nu^2)\delta\omega^2/386.4}{E[8+(3+\nu)a]}$$

$$m_1 = -\frac{a}{2} - \sqrt{\frac{a^2}{4} - a\nu + 1}$$

$$m_2 = -\frac{a}{2} + \sqrt{\frac{a^2}{4} - av + 1}$$

A and B are constants which are found by setting σ_r equal to its known value of zero at the bore ($r = 2.0$) and at the rim ($r = 10.0$) and solving the two resulting equations simultaneously for A and B .

The results calculated using the theoretical formulae are plotted in Figure A4 on the same axes as the results of the finite element analysis. There is slightly more difference between the two sets of results in this benchmark case than in the case of the disc of uniform thickness but, given that the finite element mesh used is fairly coarse, they are close enough (typically within 3%) to give confidence in the application of the finite element analysis. The largest difference occurs at the bore of the disc where the finite element analysis has trouble coping with the very steep stress gradient. Refining the mesh in this region would reduce this inaccuracy.

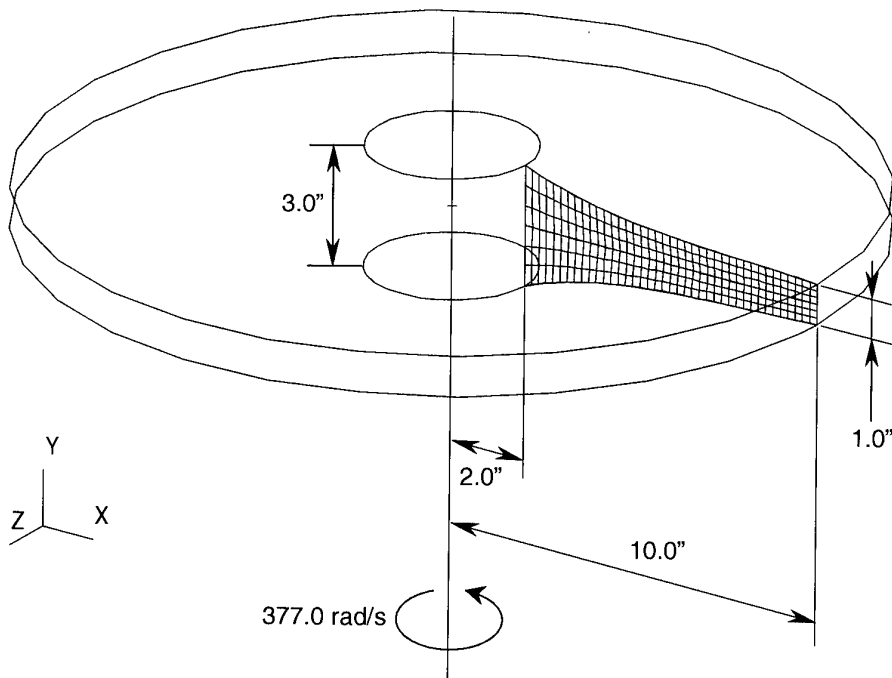


Figure A3. The geometry and mesh for the disc with hyperbolic thickness.

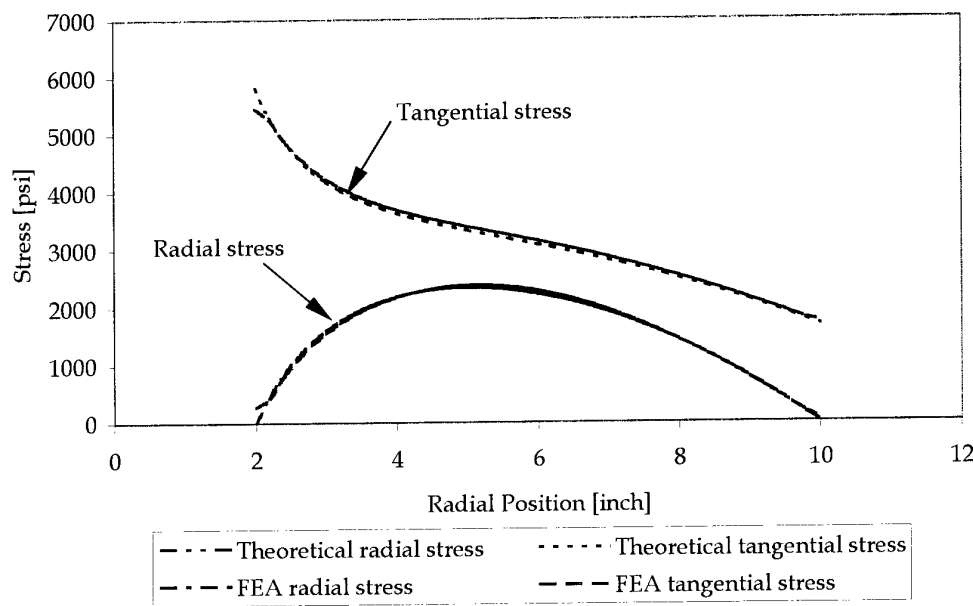


Figure A4. Comparison of theoretical and FEA stress results for the rotating annular disc with hyperbolic thickness profile.

DISTRIBUTION LIST

Preliminary Finite Element Analysis of a Compressor Disk in the TF30 Engine

J.S. Faragher and R.A. Antoniou

AUSTRALIA

DEFENCE ORGANISATION

Task Sponsor DAIRENG-SCI4A

S&T Program

Chief Defence Scientist
FAS Science Policy
AS Science Corporate Management } shared copy
Director General Science Policy Development
Counsellor Defence Science, London (Doc Data Sheet)
Counsellor Defence Science, Washington (Doc Data Sheet)
Scientific Adviser to MRDC Thailand (Doc Data Sheet)
Scientific Adviser Policy and Command
Navy Scientific Adviser (Doc Data Sheet and distribution list only)
Scientific Adviser - Army (Doc Data Sheet and distribution list only)
Air Force Scientific Adviser
Director Trials

Aeronautical and Maritime Research Laboratory

Director

Chief of Airframes and Engines Division
Research Leader Propulsion
Task Manager - Bryon Wicks
Manfred Heller
Chun Wang
Richard Callinan
Frank Skidmore
John Faragher (2 copies)
Ross Antoniou
Gordon Stocks
Jianfu Hou
Sonya Slater
Joanna Kappas

DSTO Library and Archives

Library Fishermens Bend
Library Maribyrnong
Library Salisbury (2 copies)
Australian Archives

Library, MOD, Pyrmont (Doc Data sheet only)
*US Defense Technical Information Center, 2 copies
*UK Defence Research Information Centre, 2 copies
*Canada Defence Scientific Information Service, 1 copy
*NZ Defence Information Centre, 1 copy
National Library of Australia, 1 copy

Capability Development Division

Director General Maritime Development (Doc Data Sheet only)
Director General Land Development (Doc Data Sheet only)
Director General C3I Development (Doc Data Sheet only)
Director General Aerospace Development

Army

ABCA Office, G-1-34, Russell Offices, Canberra (4 copies)
SO (Science), DJFHQ(L), MILPO Enoggera, Queensland 4051 (Doc Data Sheet only)
NAPOC QWG Engineer NBCD c/- DENGRS-A, HQ Engineer Centre Liverpool Military Area, NSW 2174 (Doc Data Sheet only)

Air Force

CENG 501 WING AMBERLEY
OIC ENGSPT 501SRLMSQN

Intelligence Program

DGSTA Defence Intelligence Organisation
Manager, Information Centre, Defence Intelligence Organisation

Corporate Support Program

OIC TRS, Defence Regional Library, Canberra

UNIVERSITIES AND COLLEGES

Australian Defence Force Academy
Library
Head of Aerospace and Mechanical Engineering
Serials Section (M list), Deakin University Library
Senior Librarian, Hargrave Library, Monash University
Librarian, Flinders University

OTHER ORGANISATIONS

NASA (Canberra)
AGPS

OUTSIDE AUSTRALIA

ABSTRACTING AND INFORMATION ORGANISATIONS

Library, Chemical Abstracts Reference Service
Engineering Societies Library, US
Materials Information, Cambridge Scientific Abstracts, US

Documents Librarian, The Center for Research Libraries, US

INFORMATION EXCHANGE AGREEMENT PARTNERS

Acquisitions Unit, Science Reference and Information Service, UK

Library - Exchange Desk, National Institute of Standards and Technology, US

National Aerospace Laboratory, Japan

National Aerospace Laboratory, Netherlands

SPARES (5 copies)

Total number of copies: **63**

| | | | |
|---|------------------------------|---|----------------------------------|
| DEFENCE SCIENCE AND TECHNOLOGY ORGANISATION DOCUMENT CONTROL DATA | | 1. PRIVACY MARKING/CAVEAT (OF DOCUMENT) | |
| 2. TITLE Preliminary Finite Element Analysis of a Compressor Disk in the TF30 Engine | | 3. SECURITY CLASSIFICATION (FOR UNCLASSIFIED REPORTS THAT ARE LIMITED RELEASE USE (L) NEXT TO DOCUMENT CLASSIFICATION) Document (U) Title (U) Abstract (U) | |
| 4. AUTHOR(S) J.S. Faragher and R.A. Antoniou | | 5. CORPORATE AUTHOR Aeronautical and Maritime Research Laboratory PO Box 4331 Melbourne Vic 3001 Australia | |
| 6a. DSTO NUMBER DSTO-TR-0915 | 6b. AR NUMBER AR-011-166 | 6c. TYPE OF REPORT Technical Report | 7. DOCUMENT DATE January 2000 |
| 8. FILE NUMBER M1/9/575 | 9. TASK NUMBER AIR 97/104 | 10. TASK SPONSOR DGTA | 11. NO. OF PAGES 38 |
| 13. DOWNGRADING/DELIMITING INSTRUCTIONS | | 14. RELEASE AUTHORITY Chief, Airframes and Engines Division | |
| 15. SECONDARY RELEASE STATEMENT OF THIS DOCUMENT <i>Approved for public release</i> | | | |
| OVERSEAS ENQUIRIES OUTSIDE STATED LIMITATIONS SHOULD BE REFERRED THROUGH DOCUMENT EXCHANGE, PO BOX 1500, SALISBURY, SA 5108 | | | |
| 16. DELIBERATE ANNOUNCEMENT No Limitations | | | |
| 17. CASUAL ANNOUNCEMENT Yes | | | |
| 18. DEFTEST DESCRIPTORS fatigue life, finite element analysis, stress analysis, gas turbine engines, fractography, fatigue tests | | | |
| 19. ABSTRACT AMRL has been developing expertise in finite element analysis (FEA) of engine components, particularly compressor and turbine discs. The fourth stage Low Pressure Compressor (LPC) disc of the TF30 engine in the F-111 aircraft was chosen as the first component for detailed analysis after being identified as a prime candidate for the retirement-for-cause lifting methodology. This report describes a preliminary study of the stresses in this component. Two benchmark examples which show close agreement between FEA stress results and analytical solutions are presented. The FEA results confirm the critical location for low cycle fatigue failure specified by the OEM. The assembly loads are shown to significantly increase the mean and peak stresses but not the cyclic stress range. The thermal stresses are shown to be an order of magnitude smaller than the stresses caused by the rotation of the disc. The analysis shows that the most severe stresses produced in the disc under typical engine operating conditions are much lower than the yield stress of the disc material (Ti-8-1-1), which suggests a very conservative design. Recommendations are made for developing models that will more realistically represent the loads on the disc and the interaction with other components in order to determine whether the design is really as conservative as the current analysis suggests. | | | |